Title
How Frequent Will the Rarest Daily Rainfall Records of Hurricane Ida’s Remnants Be in the Future?

Journal
Journal of Hydrometeorology, 27(3)

ISSN
1525-755X

Authors
Dollan, Ishrat J
Reed, Kevin A
Wehner, Michael F
et al.

Publication Date
2026-03-01

DOI
10.1175/jhm-d-25-0088.1

How Frequent Will the Rarest Daily Rainfall Records of Hurricane Ida's Remnants Be in the Future?

Ishrat J. Dollan[1], Kevin A. Reed[1], Michael F. Wehner[2], and Naresh Devineni[3]

[1]School of Marine and Atmospheric Sciences, Stony Brook University, Stony Brook, NY, USA

[2]Applied Mathematics and Computational Research Division, Lawrence Berkeley National Laboratory, CA, USA

[3]Department of Civil Engineering, The City University of New York (City College), NY, USA

Corresponding author: Ishrat Dollan (ishratjahan.dollan@stonybrook.edu)

ABSTRACT

Gaining continued insights into the impact of global warming on the hurricane-associated occurrence of intense record downpours is essential for building climate resilient communities. This study investigates projected future changes of extreme rainfall over the Northeast United States as represented by extreme daily amounts during Hurricane Ida in 2021. We used historical control simulations of Weather Research and Forecasting (WRF) generated from 40 years of weather events (1980-2014, 12 km) forced by the European Centre for Medium-Range Weather Forecasts Reanalysis version 5. These simulations are thermodynamically modified (2060-2100) via an imposed warming for the high emissions scenario of shared socioeconomic pathway (SSP585) from a range of general circulation models. Ground observations from the Global Historical Climatology Network (1950-2014) and WRF simulations (historical, 1980-2014 and future, 2060-2100) are integrated into a non-stationary generalized extreme value (GEV) framework to assess the frequency of Ida's heaviest daily rain rates under SSP585 scenario. Results show that Ida's daily maximum rainfall recorded at different observation locations was higher than the single highest September daily maximum observed (1950-2014) for 5 out of 17 stations (~30% of the stations). Ida-like daily extreme daily rain rates are projected to be more than 2 times, on average, more likely to occur at the end of the century in the simulations (with some regions as high as 5 times). This work demonstrates that integrating a high-resolution atmospheric model's present-day and thermodynamically modified future simulations, along with ground observations, within a non-stationary statistical framework, is crucial for understanding changing characteristics of extreme weather events.

Significant Statement

Daily scale extreme precipitation is expected to become more frequent and severe, as evidenced by observations and model simulations. While it is important to investigate how these intensifying heavy rainfall events affect current engineering standards, fewer studies have contextualized how warming impacts the most extreme rainfall from a single storm event relative to historical heavy downpours. In this study, we focused on the daily extreme rainfall associated with the extratropical transition of Hurricane Ida, particularly over the northeastern United States—some of which exceeded the commonly used hydrologic design criteria for a 100-year storm. Using a high-resolution atmospheric model simulation, we investigated how continued warming may influence the frequency of such daily rain rates. Under a high emission scenario, these events are projected to become up to 5 times more likely at the end of the 21st century.

1. Introduction

Understanding how record-breaking rainfall from hurricanes and how present-day and future climate change influences these ~~-~~events, requires reliable future projections. Such projections must account for a range of uncertainties across~~t~~ scales and enable estimation of plausible likelihood of these extremes. Rain rates from tropical cyclones (TCs) are projected to increase in a warmer climate (IPCC, 2023; Knutson et al., 2020; Stansfield et al., 2020; Wehner et al., 2018; Wright et al., 2015). Kunkel et al., (2010) highlighted an increase in the percentage of observed number of heavy rainfall events to TCs in the latter decades of the 20th century, which are associated with compound hazards, such as, high winds, storm surges, and coastal and inland flooding (Bhuiyan et al., 2024; Gori et al., 2022; Peduzzi et al., 2012). Our study examines rainfall of Hurricane Ida (2021), a landfalling storm that tracked from Louisiana to the northeast (NE) and brought heavy rainfall on September 1st and 2nd in the NE, exceeding climatological annual maxima recorded at several stations. According to the National Hurricane Center's report on Ida, the extratropical transition occurred after 1200 UTC on September 1st in Tennessee Valley, and the transition continued to move east-northeastward following the mid-latitude westerly wind (Beven II, et al., 2022). Using WSR-88D (Weather Surveillance Radar—1988 Doppler) polarimetric radar fields Smith et al., (2023) documented that Ida's rainfall in the Northeast exceeded the 1000-year return levels for short-duration (~1–3 hr) accumulations. Menemenlis et al., (2024)~~-~~ underscored the role of Ida's extratropical transition in amplifying these extremes and causing record ~~-~~flooding.

Studies examining long-term trends of intensity and frequency of multi-duration events, ranging from hourly to multi-day over NE (Crossett et al., 2023; Jong et al., 2023) demonstrate that warming influences extremes, making them more intense (O'Gorman, 2015; Prein et al., 2017; Rahat et al., 2024). Extreme precipitation days in the observations are becoming more frequent in the mid-Atlantic and the NE of the United States (Henny et al., 2023). The increasing trends of regional rainfall have~~s~~ been linked to higher financial costs from flood damage (Davenport et al., 2021). Using the SPEAR (Seamless system for Prediction and EArth system

Research) climate model with a resolution of 25 km, Jong et al., (2023) showed that the frequency of the top 1% daily autumn rainfall will double by the end of the century in NE. An earlier study by Huprikar et al., (2023) that focused on a storyline analysis of Hurricane Irma rainfall over Florida showed a simulated increase of 16-26% average accumulated rainfall per degree Celsius (Kelvin) under future climate warming. Studies have also demonstrated that the contribution of TCs to heavy downpours along with storm surge (Howarth et al., 2019; Kunkel et al., 2020) can lead to compound flooding along the U.S East and Gulf coasts (Ali et al., 2025; B. Jong et al., 2024; Smith et al., 2023). A study from 1998 to 2016 using satellite estimates from Tropical Rainfall Measuring Mission and Global Precipitation Measurement missions (Guzman & Jiang, 2021) attributes a 1.3% annual upward trend in average rain rate from TCs at a global scale. The authors highlighted the more pronounced trend of the average rain rate in the North Atlantic and Northwestern Pacific (Guzman & Jiang, 2021). In a statistical analysis, ~~(~~Risser et al., (2024) examined in situ seasonal mean and extreme contiguous United States (CONUS) precipitation to isolate the effects of natural and anthropogenic forcing agents. The authors found that substantial increases in NE extreme precipitation during hurricane season were partially offset by cooling from sulfate aerosol prior to the passage of Clean Air Acts in the early 1980s. Collectively, these studies highlight a growing tendency toward more frequent and intense rainfall extremes in the NE. In addition to the observed trends, tropical cyclones make a large contribution to heavy rainfall events in the region (Huang et al., 2018, 2021; Murakami et al., 2018).

Record rainfall events from tropical storms require modeling at finer spatial scales, which conventional general circulation models (GCMs) often fail to capture due to inadequate resolutions (100-250 km) and poorly resolved processes (Emanuel, 2021). Alternatively, model improvements in the representation of km scale processes and extremes on climate timescales in efforts such as the High Resolution Model Intercomparison Project (HighResMIP) with relatively finer resolution GCMs (<=50 km) are possible, but are highly computationally intensive (Haarsma et al., 2016; Roberts et al., 2025). However, different bias-correction techniques applied to GCMs for studying extreme precipitation can be grouped into statistical and dynamical (Alam et al., 2018; Moradian et al., 2024), each introducing challenges, such as overfitting from the use of many parameters (Mehrotra & Sharma, 2021). Statistical bias-correction, leverage statistical relationship between model simulations and observed rainfall, applied to the mean, variance or different quantiles (Cannon, 2018; Li et al., 2014; Maraun, 2013). While statistical bias-correction has been shown to improve modeled rainfall during historical periods, time-invariant bias adjustments extrapolated into the future fail to account for changes in dynamical processes (Mehrotra & Sharma, 2021), or for the physical processes missing from the models that may have originally caused the biases. Thermodynamic modifications of dynamically downscaled high resolution model reanalysis products are shown to be useful in studying characteristics of extreme events (Cannon & Innocenti, 2019; Jorgensen & Nielsen-Gammon, 2024). These modifications commonly referred to as "pseudo-global warming" or 'imposed global warming" (Schär et al., 1996), involve perturbing the initial and boundary conditions of the simulation to represent a warmer (or cooler) climate. These model runs can generate different climate responses to an observed event and make what-if scenarios about event magnitude and scale. In this context, these model runs can be used to characterize event-scale risk in different climates, referred to as 'storylines' in the literature (Armon et al., 2022; Hazeleger et al., 2015; Reed et al., 2020; Shepherd et al., 2018). While storyline simulations are computationally efficient, they presume that large scale circulation factors remain unchanged across simulations. Thus, to help enable climate-informed decisions and resilient infrastructure planning, it is essential to also examine the probability of rare events under future climates. Storylines focus on a given event and are not designed to infer its probability (Reed & Wehner, 2023). To bridge this gap, one could couple storyline experiments with probabilistic extremes analysis using dynamically downscaled, high-resolution model datasets to estimate the likelihood of low-probability, high-impact rainfall events (Araujo et al., 2022; Innocenti et al., 2019; Zorzetto et al., 2016).

Building on these approaches, many studies translate projected changes into design-relevant metrics, most notably percent shifts in 100-year return levels by comparing future and historical simulations of GCMs or their downscaled products (Coelho et al., 2022; DeGaetano & Castellano, 2017; Martel et al., 2021; Ragno et al., 2018). These studies typically apply extreme value analysis to estimate change factors between future and historical simulations, which are then used to adjust historical design rainfall. In doing so, they assess how the magnitude of common extremes (e.g., 10-, 20-, 50-, and 100-year return periods for 24-hour durations) may change when observational records are modified using these adjustment factors (Emmanouil et al., 2023; Tyralis et al., 2019). While this body of work has advanced our understanding of the increasing trends in common extremes (Asadieh & Krakauer, 2015; Dollan et al., 2022; Pendergrass & Knutti, 2018; Uehling & Schreck, 2024), the characteristics of rare, record-breaking rainfall events under climate change remain far less understood. Despite broad consensus that upper-tail precipitation has intensified across regions, substantial uncertainties persist in how climate change may shape the likelihood and severity of unprecedented rainfall extremes (Moustakis et al., 2021; Wang et al., 2014).

To address this gap, nonstationary modeling approaches allow us to account for climate change induced shifts in heavy rainfall by incorporating covariates such as climate modes and hydroclimatic variables (Slater et al., 2021; Vasiliades et al., 2015; Vu & Mishra, 2019). Building on this framework, Mossel et al., (2024) assessed increasing future risk of the maximum hourly rainfall from Ida in New York City under the SSP126 and SSP370 emission scenarios. Their approach incorporated two different covariates, including average temperature and cooling degree day (CDD), to model intense hourly rainfall. While their study emphasized the near- to medium- term the risk of hourly extremes conditioned on average temperature and CDD, our work extends this perspective by investigating frequency of Ida-like daily extremes projected towards the end of the century under long-term climatic forcing (external explanatory variable) across a greater spatial extent beyond New York City. This broader context is consistent with previous studies that have documented increasing extremes at both hourly and daily scales across the US, with higher detectable trends observed in the daily extremes at ground stations than in hourly extremes (Barbero et al., 2017).

To this end, our study investigates the shifting probability of occurrences of rare extreme daily rainfall (i.e., Ida's extratropical stage in the NE) by leveraging a high-resolution downscaled regional model and ground-based observations. To study future changes of Ida's daily extreme we incorporated thermodynamically modified future projections of the downscaled simulations. This study aims to address the following research questions; 1) How rare was Ida's daily accumulated rainfall over the NE US in the observational records? 2) How often may this daily accumulated rainfall occur at the end of the 21st century (2060-2100)? To address the research questions, our study examines the daily maximum accumulated rainfall in observations and radar estimates. Additionally, we model the occurrence probability of Ida-like daily maximum rainfall recorded from ground observations and investigate its likelihood in thermodynamically (temperature and moisture) modified WRF simulations (referred to as thermodynamic global warming approach, or TGW; (Jones et al., (2023) representing potential future climate. Ground observations from the Global Historical Climatology Network (1950-2014) and WRF historical (1980-2014) and future simulations are integrated into a non-stationary generalized extreme value (GEV) framework to assess the frequency of Ida's heaviest daily rain rates under plausible future scenarios. Since GEV models are probabilistic tools for estimating the likelihood of extreme events, fitting different datasets to separate GEV models allows us to estimate how the probability of extremes shifts from one climatic period to another.

We studied an area at station specific level that received heavy rainfall from the same weather system, for our case the extratropical stage of Ida (2021). While we focused our study for a single event, it contextualizes Ida-like daily rainfall with the historical rainfall in these locations in the nonstationary GEV framework. Additionally, it investigates the impact of global mean radiative forcing on the extremity of the daily scale event. Although our study focuses solely on daily extremes, it complements the existing literature on hourly extremes by offering insights into how projected daily-scale risks evolve across scenarios.

The paper is structured as follows: section 2 explains observational, radar and WRF historical and future TGW simulations; and methodological description for frequency estimation of daily maximum rainfall from Ida in the NE; section 3 shows rainfall characteristics at the observation stations as well as performance of the historical simulations of WRF in terms of correlation and bias with those observations. Additionally, this section shows results on the shifting distribution of the probability of occurrence of Ida-like storm rainfall in future; and lastly section 4 discusses the usefulness of the study and draws conclusion on the properties of Ida-like storm rainfall.

2. Materials and Methods

a. Global Historical Climatology Network (GHCN)-Daily

The Global Historical Climatology Network (GHCN)-Daily precipitation dataset for 17 stations from 1950 to 2014 is used in the study. These stations shown in Figure 2A cover the NE region which received the highest accumulation during Ida's extratropical transition. GHCN-daily datasets serve as a repository for historical daily (24-h summary) weather data covering 80000 global stations (Menne et al., 2012). Integration from different national networks such as National Oceanic and Atmospheric Administration/National Climatic Data Center (NOAA/NCDC), Global Climate Observing System (GCOS) program, European Climate Assessment and Dataset are encoded in maintaining the daily climate summaries (Menne et al., 2012). These stations are retrieved from different sources with their name, location, and daily sample criteria.~~-~~ For station pairs from the same source with ≥ 50% record identity and documented proximity (≤ 40 km), the longer record is retained for inclusion (Menne et al., 2012). Station information is also cross-checked with network affiliation (Menne et al., 2012). For this work we selected NE Stations based on a quality control process that filters out the stations with an insufficient percentage of data points, maintaining at least 80% coverage (allowing up to 20% missing values) over the 69-year historical record used for this work. If a station meets these criteria, the annual maximum is identified for each year. The 80% coverage is applied based on the assumption that there are few missing values in each year which still allow the extraction of the annual maximum value, instead of relying only on years with complete samples to avoid reducing sample sizes. However, we note that sometimes the missing values are due to intense storms which could lead to overestimation of the rarity of Ida-like events. Nonetheless, GHCN station datasets have been extensively used for analyzing long-term trends in extremes from different weather types (Henny et al., 2023; Huang et al., 2021; Risser et al., 2024). GHCN datasets provide us with long-term annual series to be used in estimating reliable rainfall for higher return periods (Cook et al., 2017).

b. Stage IV ~~-~~p~~P~~recipitation d~~D~~ata-h~~H~~ourly

Stage IV is a multi-sensor precipitation product of National Centers for Environmental Prediction (NCEP), produced at 4km/hourly spatial and temporal scales and available from 2002 to present (Lin & Mitchell, 2005). The dataset is further gauge corrected by 12 CONUS River Forecast Centers (RFCs) (Lin & Mitchell, 2005). Stage IV is used as a reliable reference in evaluating other precipitation products as demonstrated in earlier studies (Beck et al., 2019; Sharif et al., 2020). Our study utilizes the in-situ observed rainfall and WRF model simulations to estimate frequency of Ida's daily maximum rainfall in NE. However, Stage IV data is included primarily to depict the spatial pattern of rainfall from Ida in the Northeast, highlighting both the locations of the heaviest rain and its overall distribution. Daily accumulated rainfall is derived by aggregating hourly accumulation.

c. Thermodynamic Global Warming (TGW) Weather Research Forecasting (WRF)

We have used a dynamically downscaled European Centre for Medium-Range Weather Forecasts version 5 reanalysis (ERA5) in our study, developed by Jones et al., (2023). The authors downscaled ERA5 using Weather Research Forecasting (WRF) model at 12 km with 3-hour intervals. The historical simulations span from 1980 through 2019 (Jones et al., 2023). Future projections are generated by introducing thermodynamic warming, which involves applying climate change signals to the 40 year sequence of WRF simulations (Jones et al., 2023). The warming signals are derived from Phase 6 of CMIP participating in GCMs and shared socioeconomic pathways. The GCMs are selected based on their ranking in terms of skill and data availability over CONUS. The ranked models are further categorized into sensitivity groups, such as high and low, depending on their projected ensemble mean change in average temperature of CONUS for SSP585. The procedure of generating change signals in temperature and relative humidity of the future periods for the TGW WRF are as follows: 1) Remapping of ensemble members to 1 degree latitude-longitude resolution and interpolating to ERA5 pressure levels, 2) Applying 11-year moving average for the month of interest from 1979 to 2099 which eventually are adjusted as the period approaches to 2100. The monthly change is calculated per year between the periods 2019-2059 and 2059-2099 based on the reference year in the period 1979-2019. 4) The signals are interpolated from a spatial resolution of approximately 100 km to 12 km (WRF grid) and from monthly to 3-hourly, before being added to the meteorological files of the same temporal resolution for WRF model. Jones et al., (2023) evaluated the WRF historical simulations of precipitation with reference datasets using average and extreme indices. The authors found a dry bias (~< 2 mm/day) in the climatological daily maximum (average of daily maximum from 1981-2019) rainfall during spring and winter and a wet bias (~< 2 mm/day) in summer over Northeast when compared with Parameter-elevation Regressions on Independent Slopes Model (PRISM). Jones et al., (2023)- tested accumulated rainfall from Hurricane Irma between September 9, 00Z and September 12, 2017, 00Z in WRF simulations against CPC Global Unified Gauge-Based Analysis of Daily Precipitation observations and found reasonable agreement along western and central Florida. Additionally, in a recent study (Srivastava et al., (2023) evaluated the 12-km WRF simulations against the 4-km Stage IV dataset and the Oregon State University Parameter-Elevation Regressions on Independent Slopes Model (PRISM) at subdaily (3-h) and daily (24-h) timescales. Their results showed that WRF exhibits wet biases relative to PRISM in the eastern CONUS (which includes our study area). However, the author demonstrated that WRF is able to reproduce the characteristics of 24-hour precipitation frequency more accurately than Stage IV data, which supports the suitability of analyzing daily extremes within our framework.

d. Evaluation ~~s~~Statistics

The WRF historical and future (TGW) simulations are aggregated to daily scale from 3-hourly model output. The model's grid values, and the station's geographical locations are matched based on the nearest Euclidean distance. The daily time series are extracted at these locations' representative of model's daily rainfall. The daily rainfall time series for the period is matched in time. If there is a missing daily value in the ground observations, we exclude that time step from the WRF historical time series as well. The study evaluates model's historical time series with observations from 1980-2019, considering a common window at the 17 stations. The evaluation statistics used in the study are (1) Pearson correlation coefficient, and (2) percent relative difference in ~~-~~the 95th percentile of daily rainfall between model simulations and observations.

The 95th percentile for daily rainfall is calculated considering the entire period for both observations and models and the relative difference is calculated as a ratio of the difference of the 95th percentile magnitude between model and observation and the observational value. The 95th percentile is used to understand how the model represents the historical upper quantile of the observations. The following equation is used to calculate Pearson correlation coefficient at the station locations~~s~~.

$$CC=\frac{\sum_{i=1}^{N}(W_i-\overline{W})(O_i-\overline{O})}{\sqrt{\sum_{i=1}^{N}(W_i-\overline{W})^2}\sqrt{\sum_{i=1}^{N}(O_i-\overline{O})^2}}$$

where W_i represents WRF daily precipitation estimation extracted at the stations at day i, N is the number of daily samples from 1980-2019 for both datasets, and O_i represents observation at each station. $\overline{W}$ and $\overline{O}$ are the averages of WRF and observations, respectively.

*e. Probabili*ty~~ties~~ e~~E~~*stimation*

The GEV distribution (Coles, 2001) is fitted to annual maxima rainfall for each GHCN station location, i.e., one for observations, one for WRF historical control period, two with future (with different sensitivity such as hot and cold with SSP585). The 2021 daily maximum rainfall is kept as out of sample and is not included in the GEV estimation so that it can serve as an independent test event rather than being used to estimate the GEV parameters, following earlier studies (Anzolin et al., 2024; Irving et al., 2024). Model parameters, i.e., location, scale and shape parameters are estimated by the method of maximum likelihood estimation (Paciorek et al., 2018~~a~~; Paciorek & Schervish, 2006), while radiative forcing of well-mixed Greenhouse Gases (WMGHG) is used as a covariate for location parameters to account for the anthropogenic contribution as a measure of non-stationarity of extreme precipitation. The scale and shape parameters are estimated as time-invariant whereas location parameter is modeled as a function of time-varying global mean radiative forcing. WMGHG forcing accounts for atmospheric concentrations of carbon dioxide (CO_2), nitrous oxide (N_2O), methane (CH_4), and two different halocarbons, i.e., $CFC-11$, and $CFC-12$ and a total WMGHGs forcing represents a sum of each of these concentrations. Following the procedure applied in Risser et al., (2023), the atmospheric concentrations of WMGHGs are converted into radiative forcing (Wm^{-2}) and are derived for two periods; one for historical boundary conditions (1850-2014; Meinshausen & Vogel, 2016) and SSP585 boundary condition (2015-2100; Meinshausen & Nicholls, 2018). The GEV models account for the common period with the radiative forcing for historical and future for stations (1950-2014), WRF (1980-2014), and TGW WRF (2060-2100). Studies focusing on driving factors for shifting frequency of extreme rainfall events attributed the change to anthropogenic forcing (Agilan & Umamahesh, 2017; Estrada et al., 2023). Risser et al. (2024) highlighted GHGs as a significant driving factor for increased mean and extreme rainfall at GHCN rain gauge locations and historical CMIP6 simulations in the Northeast of the United States. The study also reported statistically significant increases in all seasons, with particularly strong signals in spring and autumn. Building on previous literature, our study investigates the anthropogenic influence on daily precipitation extremes at the local scale. Extending the findings of Risser et al., (2023) who linked precipitation extreme trends to well-mixed greenhouse gases, we investigate how such forcing affects the frequency of daily extremes during a specific weather event.

The GHCN and WRF historical GEV models exclude Ida's September rainfall and builds on Ida-like record rainfall without explicitly separating storm types. The rationale for fitting GEV to annual maximum daily rainfall is to represent full distribution of extremes as opposed to isolating a single season or storm type (Van Der Wiel et al., 2017).

The equation of the cumulative distribution function (CDF) is given as

$$F\left(\varkappa_t;\mu_0,\Box_{\Box}\sigma,\xi\right)=\exp\left\{-\left[1+\xi\left(\frac{\varkappa_t-()}{\sigma}\right)\right]^{\frac{-1}{\xi}}\right\}$$

$$()\Box_{\Box}\Box_{\Box}()\Box_{\Box}$$

where $\mu_o, \mu_1, \sigma, \wedge \xi$ are base location, slope of the location, scale and shape parameters of GEV distribution and $\varkappa$ is annual maximum precipitation at time t. $RF_{WMGHG}(t)$ represents the global average of radiative forcing in Wm^{-2} from the WMGHGs at time t. The location parameter is estimated in relation to the global mean of $RF_{WMGHGs}(t)$ for specific stations.

In our study we applied probabilistic attribution of the Ida's daily maximum rainfall in the thermodynamically modified WRF simulations under SSP585. The approach uses risk ratio (RR); that is a ratio between the probability of an event for the projected simulation and the probability of the same event in the present day (Kharin et al., 2018). means the Ida-like event becomes more likely by a factor . means less likely by a factor $\frac{\Box}{\Box}$.

We estimate the probability of -daily maximum rainfall at each station location using the above -mentioned nonstationary GEV distribution. The GEV estimated probability for WRF future (for different range of GCM sensitivities to SSP585) represent Ida-like daily extreme's probability with in thermodynamically perturbed WRF simulations. The CDF of the fitted GEV distribution for GHCN station (black line) maximum daily rainfall (1950-2014), shown alongside observed station data (black circle) in Figure 1. The GEV fitting was performed using the climextRemes package (Paciorek et al., 2018). Uncertainty was quantified using a nonparametric bootstrap: the original dataset was resampled with replacement, and a new GEV was fitted for each resample (500 iterations). The shaded bounds represent 5th –95th quantiles of maximum daily rainfall obtained from bootstrap resamples. Each bootstrap sample was fitted with the radiative forcing as covariate for the location parameter (Estrada et al., 2023). For individual random samples, empirical cumulative distribution function (ECDF) is calculated. (Please see the supplementary for statistical significance and uncertainty range of the fitted GEV distribution). Additional curves show WRF historical (blue), TGW low (orange), and TGW high (red) CDFs. The schematic in Figure 1 explains the methodology on estimating the probability of occurrence of Ida-like rainfall events in future. The WRF historical and GHCN station -observed GEV fitted distributions and their 5th-95th uncertainty bounds are closely aligned. The WRF future annual daily maximum rainfall shows a shift in the distribution towards a higher end (note that the simulations are thermodynamically modified). GEV parameters fitted to the -GHCN stations were used along with the maximum daily rainfall observed during September 1 - 2, 2021 (Ida extratropical rainfall) to estimate the return period of this event in the present-day climate. -Specifically, the non-exceedance probability -$\left(P\left(X \leq \square_{\square}\right)\right.$ is calculated from the CDF of the fitted GEV evaluated at the 2021 maximum. The exceedance probability is then calculated by subtracting the exceedance probability from 1, i.e., ($\square_{\square}$, which -represents the likelihood of -an Ida-like or larger event in any given year. -The reciprocal of -this exceedance probability yields the corresponding return period. We apply quantile mapping procedures that scale the probability of an actual event from the observation's GEV to model's (here WRF) GEV. For the same Ida-like probability we estimate the event rainfall (mm) from the inverse CDF of historical control WRF simulations. Using Ida-like events from the WRF historical GEV estimate, we compute the future probability of Ida-like maximum daily rainfall from the WRF future GEV CDF (high and low sensitivity simulations of SSP585). The focus of the study is to estimate the probability of occurrence of Ida-like rainfall events in future and compare the shifting distribution between the future and the observed daily maximum. An earlier study by Jeon et al., (2016) used a quantile bias correction approach to address discrepancies between observed and modeled extremes in the context of the 2011 heatwave in the central U.S. Extending our current framework to spatially aggregated rainfall (e.g., over catchments or grid-based averages) would provide valuable insights for flood hazard assessment. Such an analysis would require methods that account for the spatial dependence of extremes, which not only necessitates high-quality gridded rainfall products or dense gauge networks but also highlights the underlying physical processes (Gründemann et al., 2023).

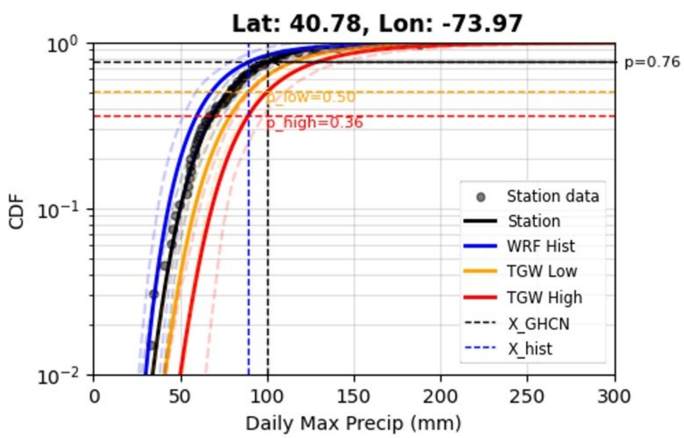

3.

Figure 1: Schematic of the cumulative probability distributions shown as an example for station at latitude 40.78 and longitude -73.97. GEV fitted lines are illustrated as solid black for GHCN, blue and dotted blue (5th and 95th bound) for WRF historical, orange and dotted orange (5th and 95th bound), and red and dotted red (5th and 95th bound) for WRF low- and high-sensitivity future simulations respectively. The black circles represent time series of annual daily maximum for 1950-2014, 1980-2014, and 2060-2100 for SSP585 respectively. The vertical black dotted line represents Ida-like rainfall event with a probability shown on the left of the figure. The vertical blue dotted line indicates WRF historical for the same Ida-like event probability. The horizontal orange and red dotted lines represent the future probability of present-day Ida-like event rainfall at daily scale

Results

a. Record r~~R~~ainfall from the r~~R~~emnants of Ida in NE and l~~L~~ong-term changes in daily maximum rainfall

First, we examined the record rainfall from both multi-day from observations and radar estimates showing multi-days (September 1st-2nd) accumulated precipitation as the storm passes over the NE in Stage IV. Clusters of accumulated rainfall for the period spreading over the region range in magnitude with some areas exceeding 200 mm shown in Figure 2. The accumulated rainfall from radar observations aligns well with the GHCN ground observations (shown as circles in Figure 2) in the region.

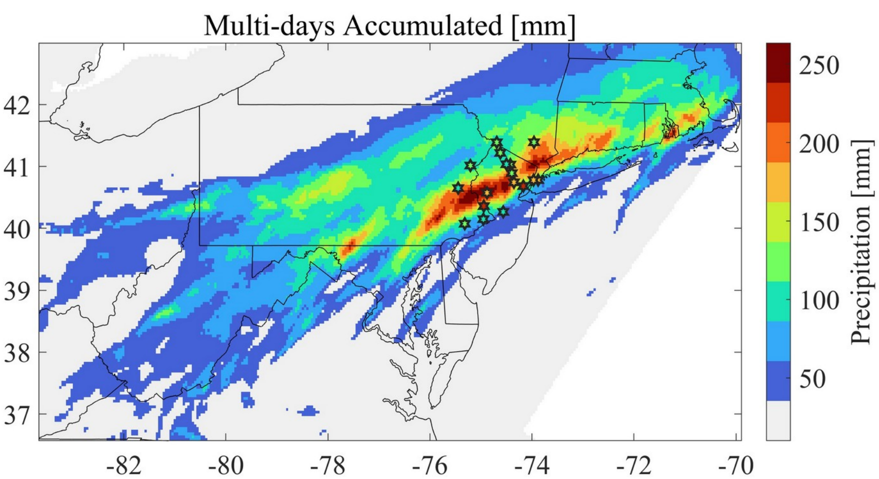

Figure 2: Multi-days accumulated rainfall in the extratropical stage of Ida from (A) Stage IV Radar and Global Historical Climatology Network - Daily (GHCN-Daily) (Sept1st 00 – Sept 2nd 18 UTC, 2021).

Figure 3 illustrates daily rainfall characteristics at the GHCN stations in the region, highlighting Ida's September maximum daily precipitation in 2021 and the single highest daily total from Septembers from 1950 to 2014. Ida's daily maximum exceeded the single highest September daily precipitation in 5 of the 17 stations included in the analysis and additional stations are close to the 1950-2014 maximum daily value. The GEV estimated 100-year return value (mean return value from bootstrapped samples) for these stations is calculated based on the annual maximum daily rainfall from 1950 to 2014 (matching with the historical period of the radiative forcing $RF_{WMGHG}(t)$).

Generally, the estimated daily rainfall with 1% chance of occurring is the highest, 3 stations exceeded even 100-year maximum daily rainfall. For a few stations, the Ida's daily maximums were closer to the 100-year return values (2 stations are within $\pm 10\%$) .Therefore, it is critical to

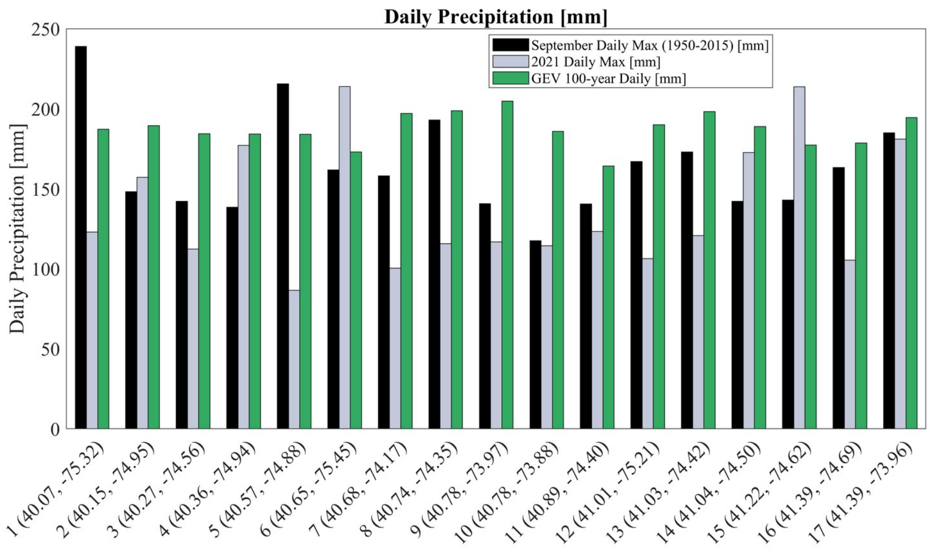

examine the frequency and intensity of such events for future scenarios.

Figure 3: Ida daily maximum in mm (light blue), climatological September maximum daily, mm (black), and GEV estimated 100-year return value (green) in mm at GHCN stations in the study area. The x axis denotes the latitude and longitude locations of the 17 GHCN stations.

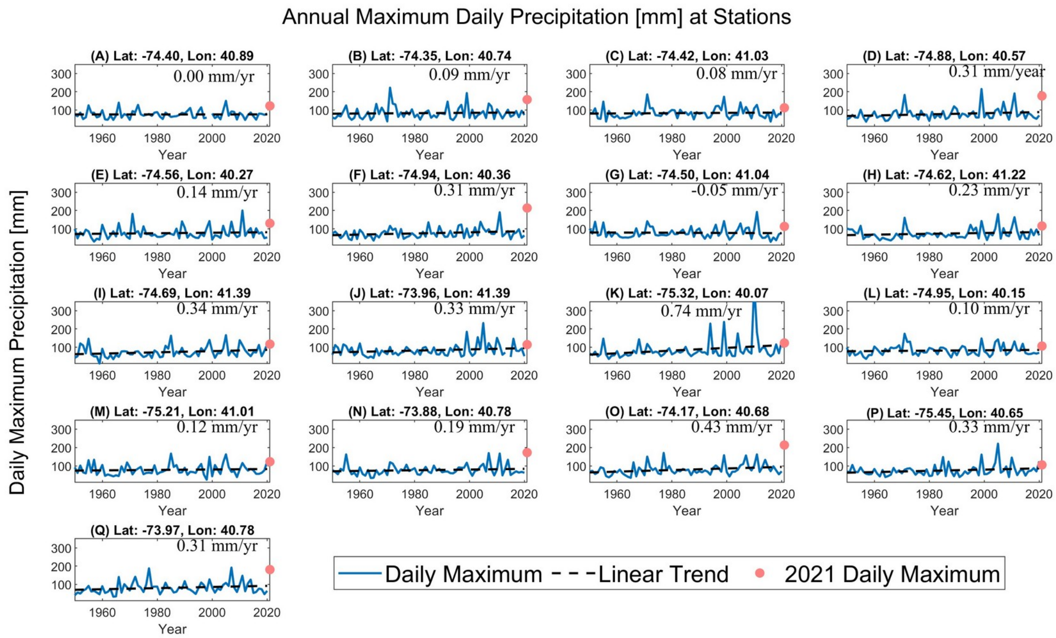

Figure 4: Time series of annual maximum daily rainfall (mm) at stations used in the study from 1950 to 2021. The dotted black line shows linear trend, and light red dot shows the maximum daily rainfall in the year 2021 at 17 stations.

Although this study centers on the characteristics of the observed record rainfall from Ida at ground stations, we additionally evaluate long-term trends in annual maximum daily rainfall at these stations shown in Figure 4 Figure 5. We estimate trends using the non-parametric Theil-Sen (TS) (Sen, 1968; Theil, 1950) and test statistical significance with the Mann-Kendall at 5% significance level (Kendall, 1948; Mann, 1945). The long-term trends were analyzed in two periods, one from 1980 through 2019 (common period with the WRF historical simulations) and the other one from 1950-2019 (shown in Figure 5). Overall, most -station exhibit small to moderate positive slope and -both the least squares method and TS agree on the sign of the trends (Figure 4 panels I, O, Q, are among statistically significant ones, alternatively GHCN identifiers USC00306774, USW00014734, USW00094728 in Figure 5 A). The statistically significant trends at the 95% confidence level are found at 5 stations for the period from 1950 (shown in Figure 5 with green cross) and onwards which is reduced to a single statistically significant station when periods from 1980 to 2020 are taken. Figure 5 B maps the station locations and the observed daily maximum from Ida's remnants (blue shading) to provide spatial context for where the most intense Ida-day totals occurred relative to the trend results in Figure 5 A. Ida's daily maximum (between September 1st and 2nd) is less than 2021's annual maximum for three stations in Figure 4 panels E (Ida September daily maximum = 86.6 mm and 2021's daily maximum = 130 mm), G (Ida September daily maximum = 100.3 mm and 2021's daily maximum = 113 mm), and M (Ida September daily maximum = 120.7 mm and 2021's daily maximum = 122.9 mm). Among the remaining stations, 9 received the annual maximum from Ida, on September 2nd, while 5 recorded their maximum on September 1st. Although Ida was rare at most stations in 2021, earlier records include daily totals comparable to or higher than Ida (Figure 4 panels D, G, J are among them). Most of these stations used in our study received rainfall of more than 100 mm in the year 2021. The linear trends are plotted for 1950 through 2020 at the stations. The trends at these stations demonstrate changes in daily rainfall time series, allowing us to investigate the nonstationary GEV model.

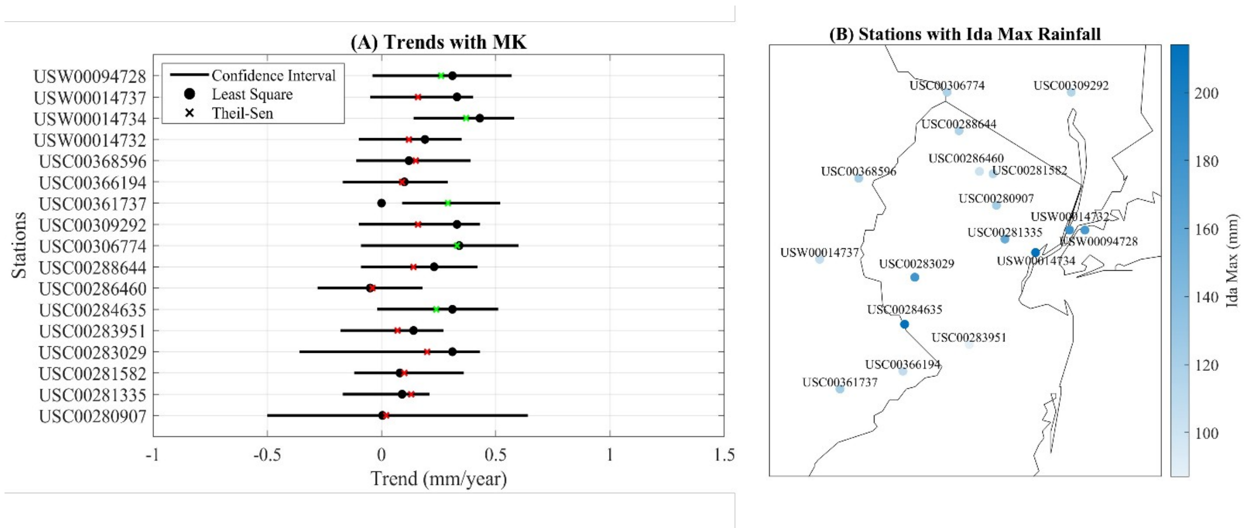

Figure 5: Long-term maximum daily rainfall trends in mm/year (1950-2020) at the 17 GHCN stations marked with the GHCN identifiers (A) The Least square linear trend is shown as black dots, Theil-Sen trends are in cross markers and represented as either green (significant at 0.5 alpha significance level tested by Mann-Kendall) or red (non-significant). The black horizontal lines for individual stations represent confidence interval calculated for TS. (B) Locations of the 17 GHCN stations. Point shading shows the observed daily maximum from Ida's remnants with darker blue to more intense daily total, and labels are the station IDs.

b. Evaluation of WRF historical control simulations with stations

The section demonstrates performance of the higher resolution WRF historical control simulations at the stations. Figure 6A shows the daily scale Pearson correlation coefficient, with values ranging from about 0.45 to 0.65, indicating a moderate skill in capturing temporal variability of daily rainfall across the region. Relatively higher values of correlation coefficients are clustered in the eastern part of the study region. In general, we found reasonable daily correlation, with values higher than 0.6 at some stations, between GHCN stations and the WRF historical control simulations. Figure 6B presents the percent relative difference in the 95th percentile between WRF and observations, calculated as $\frac{\square}{\square}$. The relative differences generally range between approximately –10% (blue shading) and +5% (red shading), with negative values indicating underestimation of the top 5% extremes by WRF and positive values indicating overestimation. This demonstrates that despite the slight underestimation of magnitude WRF is able to replicate the 95th percentile of the daily rainfall compared to ground observations.

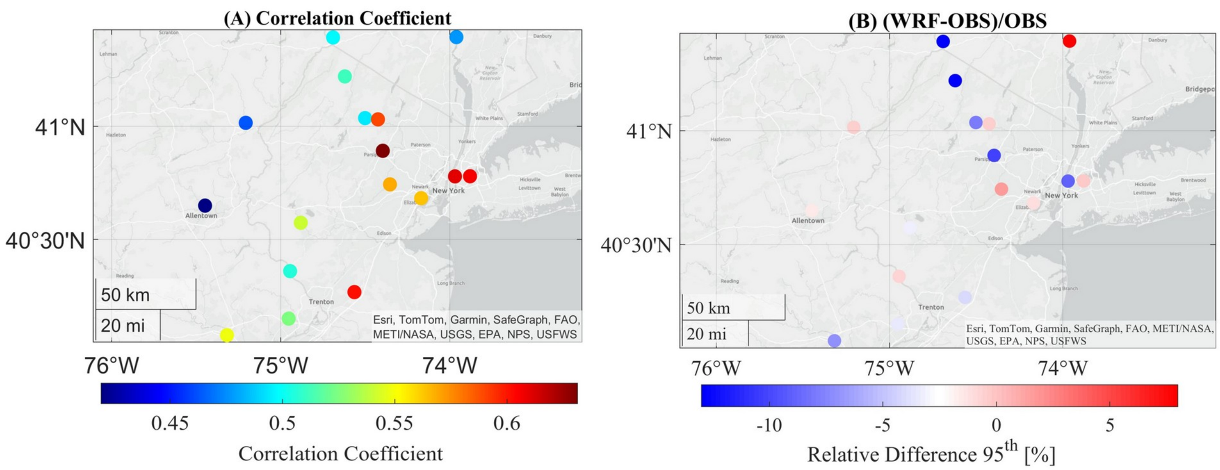

Figure 6: Performance of the WRF historical simulation compared to observations is shown in (A) Pearson correlation coefficient (unitless) (B) Percent relative difference in the 95th percentile of daily rainfall (unitless) from 1980 to 2014 at 17 stations.

c. Evaluation of nonstationary GEV models for stations and WRF simulations

A region of upper (95th) and lower (5th) percentile encapsulates the mean (50th) return level value for individual stations, calculated from fitting the bootstrapped ~~-~~samples shown in Figure 7. The m~~M~~ajority of the stations have a narrower confidence interval for lower return periods (e.g., less than 10 years). Some stations experience more intense daily rainfall (mm) for the same return periods as others, which represents regional differences in extremes. For instance, a 100-year mean return level for subplot (A) is below 200 mm, whereas subplot (B) shows a more intense return level than the station in subplot (A). Stations with steeper return level slopes demonstrate intense rainfall at daily scale.

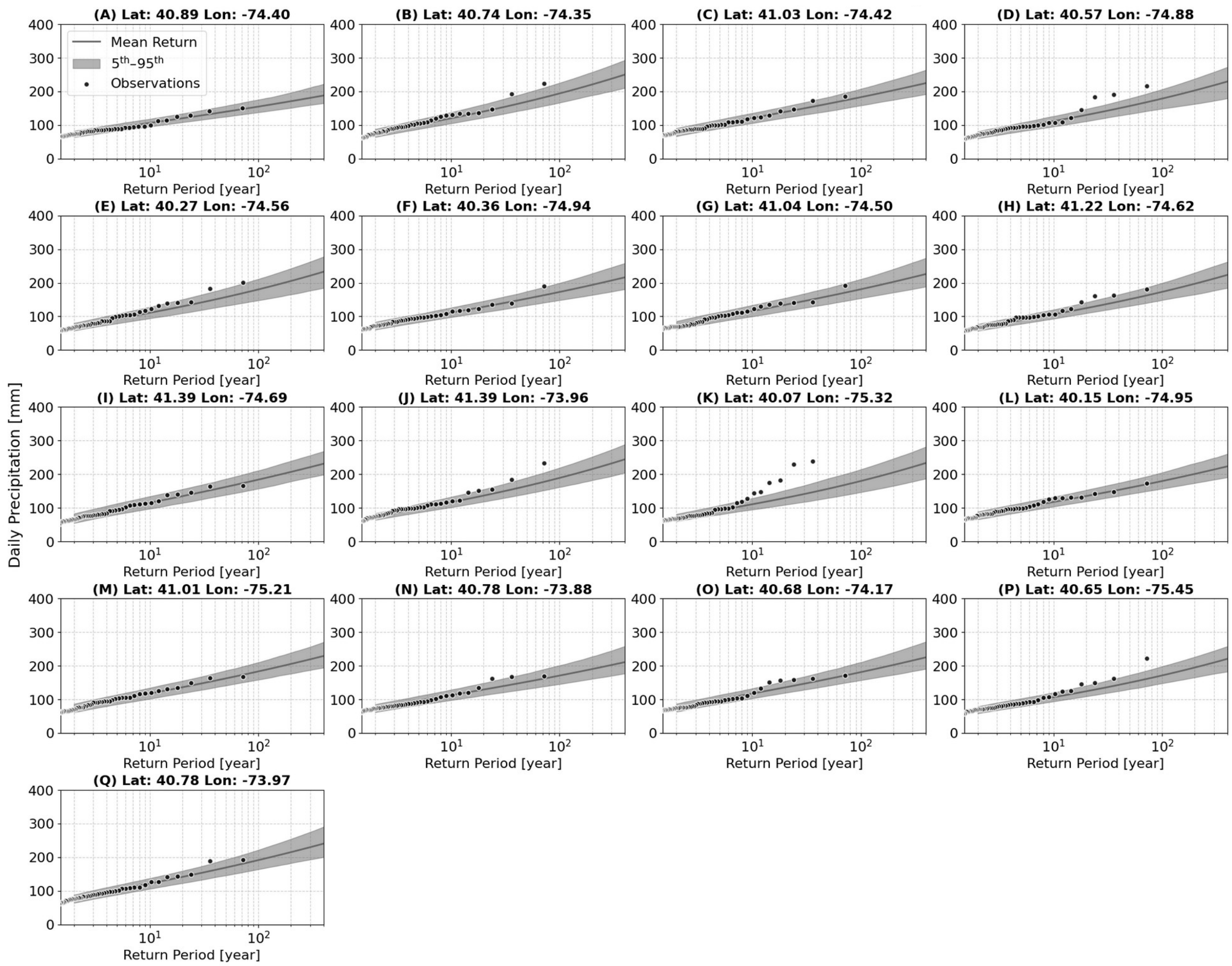

Figure 7: GEV model estimated return levels of daily maximum (mm) across different return periods at GHCN stations conditioned on the radiative forcing of well mixed greenhouse gases in 2021. The 5^{th}-95^{th} percentile range (mm) for individual stations shows GEV estimated rainfall (mm) from the bootstrapped samples. The observations samples are shown in black dots.

Next, in Figure 8 we compare how the GEV fitted WRF historical control simulation replicates the rainfall extremes with that of observations while conditioned on the 2021's radiative forcing to keep it comparable with the event year. Figure 8 also shows rainfall extremes for two future projections (low- and high-sensitivity TGW WRF simulations). The 5^{th}-95^{th} percentile interval for the historical control simulation (WRF Hist.) at different station locations has a wider spread than that of observation-based GEV estimation, particularly for higher return periods. At lower return periods, WRF historical return levels more closely match the station-based estimates across locations. However, the mean estimated rainfall (across the bootstrapped samples) for the historical simulations are in consistent agreement with the mean estimated rainfall for all stations, despite the well-known issue of differences between point measurement and gridded model precipitation (Risser et al., 2019; Timmermans et al., 2019). The goodness of the fit of the station based GEV model is evaluated with Kolmogorov–Smirnov (KS) test ("Kolmogorov–Smirnov Test," 2008) and Anderson-Darling (AD) test ("Anderson–Darling Test," 2008) (see supplementary Figure S2 and Table S1 for KS test and section b for AD test). The AD test results show that both observational and WRF-simulated datasets support the suitability of the nonstationary GEV for describing extreme rainfall, as indicated by bootstrap p-values relative to the 0.10 critical value. However, in a few cases, both the observational and WRF-based GEV fits may be inadequate due to the limited sample size.

Additionally, we included the Wilcoxon signed-rank test as a bias check on central tendency. It asks whether the median of the within-year differences (WRF – station) departs from zero. The test found no evidence that the median paired difference differs from zero (all $p > 0.05$). The uncertainty of the estimated daily precipitation from historical WRF simulations is comparable to those of the stations (see supplementary Figure S5). For instance, the 5th percentile values for station and WRF historical simulations are in close agreement for a 100-year return period. However, the 95th percentile of the WRF historical simulations overestimates the station's 95th for the same return period. At the 100-year return period, the median of the bootstrapped distributions projects higher daily rainfall amounts in the future scenarios compared to the historical GHCN baseline (see supplementary Figure S6). Figure 8 highlights (text in each panel) the percent difference between Ida's observed rainfall and the GEV estimated rainfall (average across all the bootstrap fits) corresponding to Ida's return period at each station. The differences range from –12.1% to +2.0%, indicating that the GEV model estimate tends to underestimate rainfall amounts for Ida-like events in most stations. The GEV-estimated rainfall is underestimated at all but six stations for Ida-like events.

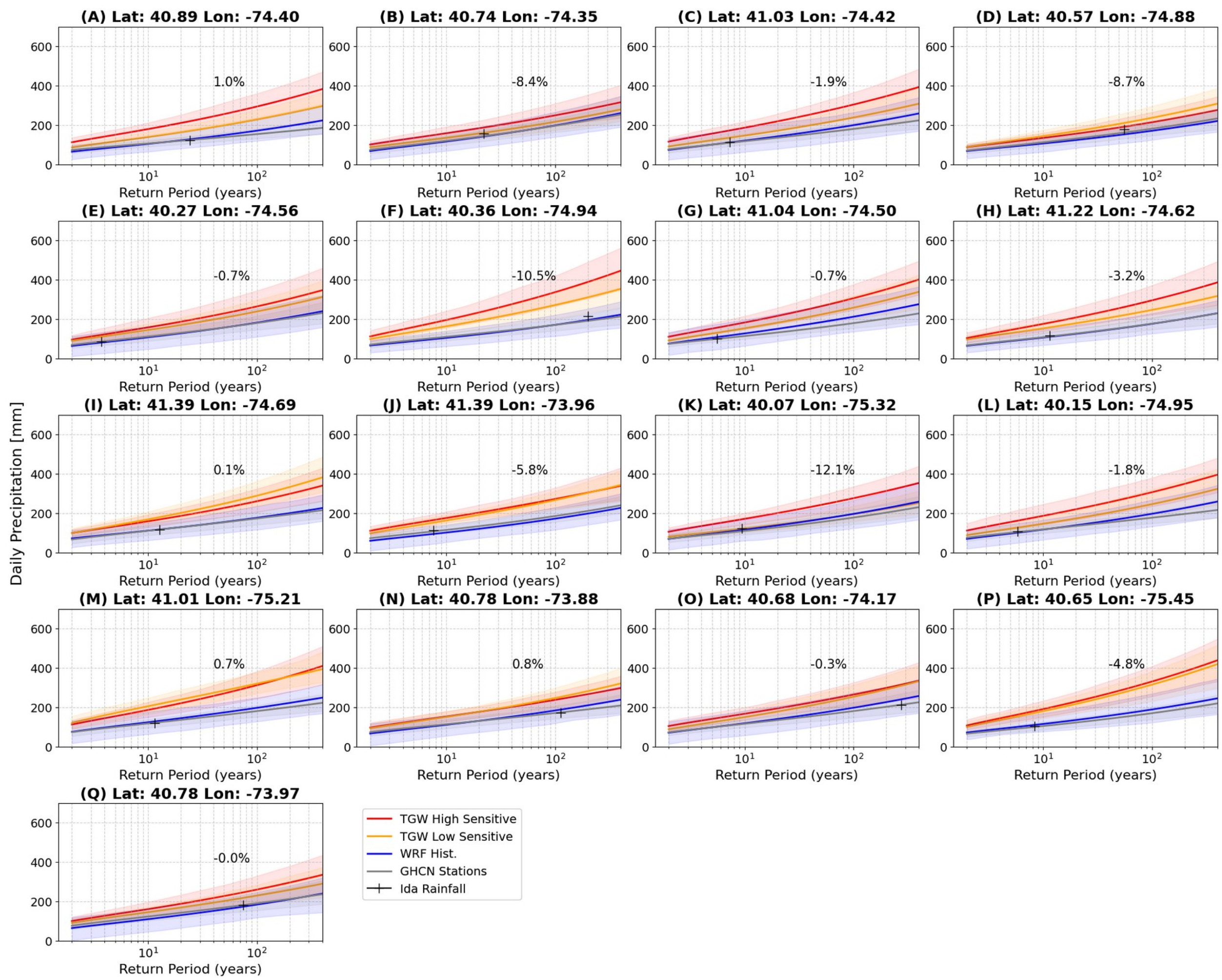

Figure 8: GEV-based return-level curves (with bootstrap uncertainty) for annual maximum daily rainfall from stations and WRF simulations, historical and TGW future (low- and high-sensitive) conditioned on the radiative forcing of well mixed greenhouse gases -(2021 and at the end of the century. The black marker shows the Ida maximum. Shaded bands show the 5^{th}-95^{th} percentiles from bootstrap resampling: TGW future high- (red), TGW future low-sensitive (orange), WRF historical (blue) and stations (gray). The solid lines represent the bootstrap means. The percentage in each panel (A-Q) shows the relative difference between the mean return level (mm) and Ida's maximum daily rainfall. The x-axis is the return period (year, log scale); the y-axis is daily precipitation (mm).

Figure 8, -provides the annual maximum daily rainfall probability distributions for low- and high-sensitivity future TGW WRF simulations (conditioned on end of century RF). In general, in the future the precipitation extremes will have a higher magnitude, as much as 400 mm/day for a

100-year event (upper bound to the high sensitivity simulation) for some stations. One exception is shown in Figure 8K, where the mean return levels of historical and TGW (low sensitivity) simulations are closely aligned at those locations. On average, 100-year daily rainfall events are projected to be approximately 36%/50% (low- and high-sensitivity) higher than the historical WRF model precipitation.

d. The future change in probability of Ida-like events

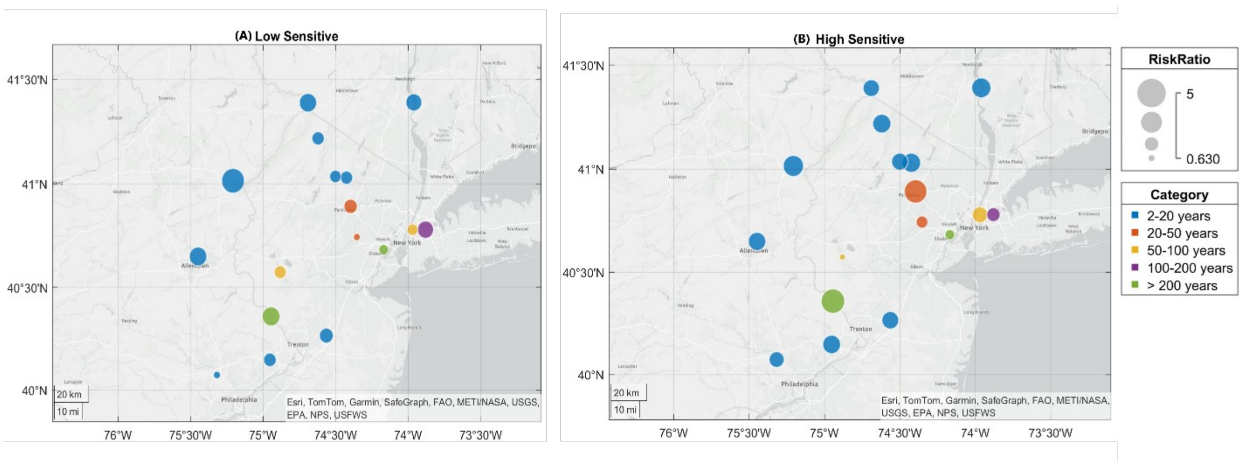

Figure 9: Future risk ratio (RR) of Ida-like maximum daily rainfall under SSP585. Stations are grouped by the present-day (2021) return period of Ida at that station (2–20, 20–50, 50–100, 100–200, >200 years). The ratios represent the change in probability of Ida-like daily maximum rainfall change induced by well mixed greenhouse gas radiative forcing at the 17 stations for (A) low- (B) high-sensitivity.

Figure 9 represents the likelihood of Ida-like maximum daily rainfall changes under the SSP585 by the end of the 21st century relative to 2021. Stations are grouped by Ida's present-day (2021) return period at each site (2–20, 20–50, 50–100, 100–200, >200 years); at some locations Ida was as rare as a 200-year event. Across stations, the risk ratio (RR = future/present likelihood) spans 0.6–5.0, i.e., from ~40% less likely (RR=0.6) to up to 5× more likely (RR=5.0), with the majority of stations RR>1. In the two stations where Ida was a 50–100-year event, RR lies near the lower end of the range in the low-sensitivity run (Figure 9A), while one of these shifts toward the upper end in the high-sensitivity run (Figure 9B). These results demonstrate that RR is below 1 in a single station with return period in the range of 20-50 years, indicating a decrease in the risk of the once in 20 to 50 years period of daily rainfall (~25% reduction) from present level. Several stations in the 2–20-year show comparatively larger relative changes in the RR. At one

New Jersey station where Ida is estimated to be >200-year in 2021 (subplot F in Figure 8), RR exceeds 1 in both TGW simulations. Generally, events that are 50-year and above are in the upper range of the RR. While rare events such as 200-year events are projected to be more frequent, the less rare extremes also show increased frequency in this region. Overall, end-of-century SSP585 conditions make 2021-Ida-like daily rainfall more likely at most stations, with upper-tail increases up to ~5 times, with a spatial average/median RR of 2.1/1.7 and 2.8/2.8 for low- and high-sensitivity respectively, across all stations. Our analysis compares exceedance probabilities of the 2021 Ida total; it does not estimate future event magnitudes.

While we show the RR range from a reasonable GEV fitting of the historical and future model simulations, it is noteworthy to mention that the estimated upper bound of the RR is much higher (as high as 9 times, not shown here). We penalized the higher value of shape parameters (to have similarities with that of observation's fit parameters) as has been discussed by Van Der Wiel et al., (2017). As heavier tail behavior causes the maximum daily rainfall distribution to shift to right which impacts risk ratio by reducing the events probability (Kharin et al., 2018). The ratio helps to compare the probability of Ida's September maximum daily maximum from present-day climate with the probability of the same event under different climate scenarios and this metric has been extensively used in earlier studies (Martinez-Villalobos & Neelin, 2023; Paciorek et al., 2018; Perkins-Kirkpatrick et al., 2022). While daily rainfall events such as the one from Ida are studied in terms of frequency for the GHCN stations daily rainfall, the high impact short duration (e.g., 1~3 hr) can also be investigated from the TGW WRF simulations in future work.

4. Discussion and Conclusions

Our study investigates the changing frequency of high-impact daily rainfall from Ida's extratropical stage in the NE US. We used GHCN ground observations, radar estimates, and 12-km resolution dynamically downscaled model simulations to evaluate the rarity of the event and to explore plausible futures in Ida-like daily rainfall extremes. Ida's multi-duration accumulated rainfall showed a cluster of cells that brought rainfall as high as 250 mm in places NJ and NY, as observed from ground observations and radars. These regions receive a maximum hourly rain of as much as 100 mm. The long-term trend of maximum daily rainfall illustrates that while Ida has the wettest spells for 2021, some of these stations received similarly high or higher daily rain rates in recent decades. Here we highlight that in recent decades, particularly after 2000, there are more peaks in the annual daily maximum observed at majority of the stations, which reflects increasing trends at these stations. We demonstrated a direct comparison of September's daily maximum (mm) at these stations with their climatological highest daily maximum (mm) and found that Ida's September maximum rainfall exceeded the climatological highest ranking in 5 stations.

Estimating reliable changes in the likelihood of extreme events under climate change requires long-term historical records as well as future climate projections at high spatial resolution (Jong et al., 2024). We modeled extreme daily rainfall within a non-stationary GEV framework without defining individual storm types. The rationale for not disentangling storm types is due to the fact that daily heavy rainfall from Ida would have impacted at the same level in terms of hazards in NE for the present-day climate, irrespective of the drivers. Additionally, statistical model's robustness such as GEV relies on a larger sample size (i.e., reliable estimations of rainfall intensity and frequency), which will be reduced if categorized storm types. However, it is worth noting that stratifying storms into different classes could uncover varying patterns of change. This risk-based framework supports case study evaluations of warming impacts on ~~ies~~ of extreme events (Tanaka et al., 2023).

Our findings corroborate to the earlier studies that highlighted increasing of frequency of daily extreme rainfall in the NE US in observations and climate models (Barlow et al., 2019; Myhre et al., 2019; Nanditha et al., 2024; Olafsdottir et al., 2021). Previous studies has analyzed extremes by applying the concept of TGW using perturbations; either thermodynamic alone or both thermodynamic and dynamic initial and boundary condition to examine storm-rainfall -across different temporal scales **(Chen et al., 2020; Olschewski & Kunstmann, 2024; Rasmussen & Liu, 2017; S. Wang & Wang, 2019; Zarzycki et al., 2024)**. Our study builds on this by employing GEV models to compare how well atmospheric models replicate daily rainfall extremes. We used the GEV fitted model to examine the plausible range of risks of rare, high-impact rainfall extremes in -perturbed simulations of WRF for different GCMs sensitivities to warming. TGW simulations used in our study inherently ignore internal climate variability, as they are perturbed from a single historical WRF simulation. Consequently, the uncertainty range is constrained by the choice of GCM sensitivity, i.e., low versus high sensitivity under the SSP585 scenario. Applying thermodynamic perturbations to multi-ensemble historical simulations would provide a broader range of uncertainties across emission scenarios. The added value of using dynamically downscaled and thermodynamically modified WRF simulations in fitting GEV models lies in the ability of the GEV framework to quantify the probability of the thermodynamic response of extreme rainfall. Particularly, we investigate how an *x*-year event in the past would manifest in a plausible warmer future climate. We find qualitatively consistent projections for the risk of daily extremes with those of **Mossel et al., (2024)** which show an increasing risk of Ida-like extremes irrespective of event scale, with risks further amplified under higher emission scenarios and when applying a non-stationary modeling approach. Our study is based on thermodynamically perturbed WRF simulations, whereas Mossel et al. employed coarse-resolution CMIP6 models (GFDL-ESM4.1, MPI-ESM1-2-HR, CESM2). In addition, higher-resolution (25 km) SPEAR (Seamless system for Prediction and EArth system Research) climate model projects daily extreme precipitation (September-November) to be more likely, e.g., six times more in the northeastern US by the end of the century (Jong et al., 2023). Despite these differences in the modeling framework and future projections as well as in definition of extremes, the collective evidence points a similar conclusion; the eastern US is becoming wetter as the most extreme rainfall events grow intense and frequent (Ali et al., 2018; Allan & Soden, 2008; IPCC, 2023), which can be influenced by local conditions at stations (Evans & DeGaetano, 2025).

Future studies should consider exploring the frequency of multi-day rainfall. The TGW future simulations for the emission scenario (i.e., SSP585) are used to compare the daily most extreme rainfall from Ida's remnants with the WRF model's long-term daily maximum. Previous studies have also emphasized the need to translate point-scale extremes into basin-scale risks. **Vohnicky et al., (2025)** demonstrated that storm rainfall characteristics, including duration and return period, can be designed as functions of basin scale, showing that areal reduction factors (ARF) decrease as storm duration increases over larger basins. This highlights how peak point rainfall totals differ substantially from basin-averaged precipitation, underscoring the importance of considering spatial dependence. As has been shown for basins in the upper Adige River system in the eastern Italian Alps, such basin-scale analyses are promising directions for extending our methodology to better capture spatial variability of extremes across diverse hydroclimatic regions.

To account for the non-stationarity in extreme precipitation due to anthropogenic climate change, we introduced greenhouse gas concentration as a covariate to the location parameter of the ~~fitted~~ GEV distribution. Confining the covariate to only the location parameter means that while the GEV distribution can shift, its width and shape is estimated as stationary. To quantify sampling and parameter uncertainties in the fitted distribution, we used a nonparametric bootstrap method as this method is robust to model complexity (**Serinaldi & Kilsby, 2015**). We have also quantified the percentage difference between Ida's observed rainfall, and the GEV estimated rainfall (average across all the bootstrap fits) corresponding to Ida's return period at each station. The differences range from -13.6 to +2.0%. Sources of GEV model uncertainty include uncertainty with parameter estimations and sample's record length, with additional uncertainties from the choice of covariate. Interpretation of the results presented in the study are due to representation of WRF's extreme subset from historical as well as future response of warming to the extreme subset. We fit the GEV models to each dataset conditioning on the radiative forcing of WMGHG as a covariate for location parameters to account for anthropogenic contribution. Despite the combined uncertainties, the nonstationary GEV fits capture the historical extremes well, and the 5^{th}–95^{th} percentile intervals encompass the observations at most stations. Results are compared between the individual GHCN weather stations and the climate model simulations. The principal research questions addressed in this study are:

1) How rare was Ida's remnant over the NE US in the observational records? Our results demonstrate that the most extreme daily rainfall from the remnants of Ida is concentrated over the NJ and NY area; the rarity of the most extreme rainfall is observed at stations exceeding even the highest ranked daily rainfall from the historical record and the 100-year daily maximum return levels. Additionally, the stations studied received a record amount of daily rainfall, showing values close to the climatological maximum for September. Results show that Ida's daily rainfall varies from a range of 2 to 300 in return periods in present-day climate. The long-term trends across these stations show that Ida-like extremes are becoming more frequent in recent decades.

2) How often does this type of event occur in future? The heaviest spells contributing to maximum daily accumulated rainfall are studied at GHCN observations. The Ida like daily extreme rain rates is projected to be more than 2 times, on average and as high as 5 times more likely to occur at the end of the century with different range of GCM sensitivities to SSP585. Instead of using coarse-resolution raw GCM outputs and our study used thermodynamically modified higher resolution regional model (WRF). Our study investigated the high emission scenario, but both high- and low-sensitivity TGW simulations show increased likelihood at stations within the study area.

Lastly, this study is an attempt to contextualize heavy rainfall from the extratropical stage of Ida from present day climate and thermodynamically perturbed future climate for the high emissions scenario. Our results show a range of increased likelihood of Ida's daily maximum rainfall across the northeastern stations, particularly NJ and NY in the later decades of the century.

Acknowledgments

This work was supported, in part, by the Department of Energy (DOE) Office of Science Award Number DE-SC0016605 'A Framework for Improving Analysis and Modeling of Earth System and Intersectoral Dynamics at Regional Scales,' and the National Science Foundation Award # AGS2244917. MFW was supported by the Director, Office of Science, Office of Biological and Environmental Research of the U.S. Department of Energy under Contract No. DE340AC02-05CH11231 under the Regional and Global Climate Modeling Program (RGCM). The authors would like to thank Mark Risser for providing insights on the calculation of radiative forcing of well mixed greenhouse gases.

Data Availability Statement

The GHCN datasets are available online https://www.ncei.noaa.gov/data/global-historical-climatology-network-daily. The GHCN datasets are download on ARGO Cluster managed by the Office of Research Computing (orc.gmu.edu) in George Mason University and using MATLAB code from the following git repository https://github.com/jjohns60/GHCN_extract.git. The NWS Stage IV precipitation analysis data is available for download at https://water.weather.gov/precip/download.php. The WRF simulations used in our study can be found online https://tgw-data.msdlive.org/downloads.

Software Availability Statement

Nonstationary GEV models are fitted using climextremes software https://pypi.org/project/climextremes/

REFERENCES

Agilan, V., & Umamahesh, N. V. (2017). What are the best covariates for developing non-stationary rainfall Intensity-Duration-Frequency relationship? *Advances in Water Resources*, *101*, 11–22. https://doi.org/10.1016/j.advwatres.2016.12.016

Alam, M., Emura, K., Farnham, C., & Yuan, J. (2018). Best-Fit Probability Distributions and Return Periods for Maximum Monthly Rainfall in Bangladesh. *Climate*, *6*(1), 9. https://doi.org/10.3390/cli6010009

Ali, H., Fowler, H. J., & Mishra, V. (2018). Global Observational Evidence of Strong Linkage Between Dew Point Temperature and Precipitation Extremes. *Geophysical Research Letters*, *45*(22). https://doi.org/10.1029/2018GL080557

Ali, J., Wahl, T., Morim, J., Enriquez, A., Gall, M., & Emrich, C. T. (2025). Multivariate compound events drive historical floods and associated losses along the U.S. East and Gulf coasts. *Npj Natural Hazards*, *2*(1), 19. https://doi.org/10.1038/s44304-025-00076-5

Allan, R. P., & Soden, B. J. (2008). Atmospheric Warming and the Amplification of Precipitation Extremes. *Science*, *321*(5895), 1481–1484. https://doi.org/10.1126/science.1160787

Anderson–Darling Test. (2008). In *The Concise Encyclopedia of Statistics* (pp. 12–14). Springer New York. https://doi.org/10.1007/978-0-387-32833-1_11

Anzolin, G., De Oliveira, D. Y., Vrugt, J. A., AghaKouchak, A., & Chaffe, P. L. B. (2024). Nonstationary frequency analysis of extreme precipitation: Embracing trends in observations. *Journal of Hydrology*, *637*, 131300. https://doi.org/10.1016/j.jhydrol.2024.131300

Araujo, D. S. A., Marra, F., Merow, C., & Nikolopoulos, E. I. (2022). Today's 100 year droughts in Australia may become the norm by the end of the century. *Environmental Research Letters*, *17*(4), 044034. https://doi.org/10.1088/1748-9326/ac58ac

Armon, M., Marra, F., Enzel, Y., Rostkier-Edelstein, D., Garfinkel, C. I., Adam, O., Dayan, U., & Morin, E. (2022). Reduced Rainfall in Future Heavy Precipitation Events Related to Contracted Rain Area Despite Increased Rain Rate. *Earth's Future*, *10*(1), e2021EF002397. https://doi.org/10.1029/2021EF002397

Asadieh, B., & Krakauer, N. Y. (2015). Global trends in extreme precipitation: Climate models versus observations. *Hydrology and Earth System Sciences*, *19*(2), 877–891. https://doi.org/10.5194/hess-19-877-2015

Barbero, R., Fowler, H. J., Lenderink, G., & Blenkinsop, S. (2017). Is the intensification of precipitation extremes with global warming better detected at hourly than daily resolutions? *Geophysical Research Letters*, *44*(2), 974–983. https://doi.org/10.1002/2016GL071917

Barlow, M., Gutowski, W. J., Gyakum, J. R., Katz, R. W., Lim, Y.-K., Schumacher, R. S., Wehner, M. F., Agel, L., Bosilovich, M., Collow, A., Gershunov, A., Grotjahn, R., Leung, R., Milrad, S., & Min, S.-K. (2019). North American extreme precipitation events and related large-scale meteorological patterns: A review of statistical methods, dynamics, modeling, and trends. *Climate Dynamics*, *53*(11), 6835–6875. https://doi.org/10.1007/s00382-019-04958-z

Beck, H. E., Pan, M., Roy, T., Weedon, G. P., Pappenberger, F., Van Dijk, A. I. J. M., Huffman, G. J., Adler, R. F., & Wood, E. F. (2019). Daily evaluation of 26 precipitation datasets using Stage-IV gauge-radar data for the CONUS. *Hydrology and Earth System Sciences*, *23*(1), 207–224. https://doi.org/10.5194/hess-23-207-2019

Beven II, J. L., Hagen, A., & Berg, R. (2022). *Tropical cyclone report: Hurricane Ida* (AL092021). National Hurricane Center.

Bhuiyan, S. A., Maggioni, V., Ferreira, C., & Rahman, A. (2024). A direct insertion technique to assimilate sea surface height into a storm surge model. *Journal of Hydrology*, *632*, 130886. https://doi.org/10.1016/j.jhydrol.2024.130886

Cannon, A. J. (2018). Multivariate quantile mapping bias correction: An N-dimensional probability density function transform for climate model simulations of multiple variables. *Climate Dynamics*, *50*(1–2), 31–49. https://doi.org/10.1007/s00382-017-3580-6

Cannon, A. J., & Innocenti, S. (2019). Projected intensification of sub-daily and daily rainfall extremes in convection-permitting climate model simulations over North America: Implications for future intensity–duration–frequency curves. *Natural Hazards and Earth System Sciences*, *19*(2), 421–440. https://doi.org/10.5194/nhess-19-421-2019

Chen, J., Wang, Z., Tam, C.-Y., Lau, N.-C., Lau, D.-S. D., & Mok, H.-Y. (2020). Impacts of climate change on tropical cyclones and induced storm surges in the Pearl River Delta region using pseudo-global-warming method. *Scientific Reports*, *10*(1). https://doi.org/10.1038/s41598-020-58824-8

Coelho, G. D. A., Ferreira, C. M., Johnston, J., Kinter, J. L., Dollan, I. J., & Maggioni, V. (2022). Potential Impacts of Future Extreme Precipitation Changes on Flood Engineering Design Across the Contiguous United States. *Water Resources Research*, *58*(4), e2021WR031432. https://doi.org/10.1029/2021WR031432

Coles, S. (2001). *An Introduction to Statistical Modeling of Extreme Values*. Springer London. https://doi.org/10.1007/978-1-4471-3675-0

Cook, L. M., Anderson, C. J., & Samaras, C. (2017). Framework for Incorporating Downscaled Climate Output into Existing Engineering Methods: Application to Precipitation Frequency Curves. *Journal of Infrastructure Systems*, *23*(4), 04017027. https://doi.org/10.1061/(ASCE)IS.1943-555X.0000382

Crossett, C. C., Dupigny-Giroux, L.-A. L., Kunkel, K. E., Betts, A. K., & Bomblies, A. (2023). Synoptic Typing of Multiduration, Heavy Precipitation Records in the Northeastern United States: 1895–2017. *Journal of Applied Meteorology and Climatology*, *62*(6), 721–736. https://doi.org/10.1175/JAMC-D-22-0091.1

Davenport, F. V., Burke, M., & Diffenbaugh, N. S. (2021). Contribution of historical precipitation change to US flood damages. *Proceedings of the National Academy of Sciences*, *118*(4), e2017524118. https://doi.org/10.1073/pnas.2017524118

DeGaetano, A. T., & Castellano, C. M. (2017). Future projections of extreme precipitation intensity-duration-frequency curves for climate adaptation planning in New York State. *Climate Services*, *5*, 23–35. https://doi.org/10.1016/j.cliser.2017.03.003

Dollan, I. J., Maggioni, V., Johnston, J., Coelho, G. D. A., & Kinter, J. L. (2022). Seasonal variability of future extreme precipitation and associated trends across the Contiguous U.S. *Frontiers in Climate*, *4*, 954892. https://doi.org/10.3389/fclim.2022.954892

Emanuel, K. (2021). Atlantic tropical cyclones downscaled from climate reanalyses show increasing activity over past 150 years. *Nature Communications*, *12*(1), 7027. https://doi.org/10.1038/s41467-021-27364-8

Emmanouil, S., Langousis, A., Nikolopoulos, E. I., & Anagnostou, E. N. (2023). Exploring the Future of Rainfall Extremes Over CONUS: The Effects of High Emission Climate Change Trajectories on the Intensity and Frequency of Rare Precipitation Events. *Earth's Future*, *11*(4), e2022EF003039. https://doi.org/10.1029/2022EF003039

Estrada, F., Perron, P., & Yamamoto, Y. (2023a). Anthropogenic influence on extremes and risk hotspots. *Scientific Reports*, *13*(1), 35. https://doi.org/10.1038/s41598-022-27220-9

Estrada, F., Perron, P., & Yamamoto, Y. (2023b). Anthropogenic influence on extremes and risk hotspots. *Scientific Reports*, *13*(1), 35. https://doi.org/10.1038/s41598-022-27220-9

Gori, A., Lin, N., Xi, D., & Emanuel, K. (2022). Tropical cyclone climatology change greatly exacerbates US extreme rainfall–surge hazard. *Nature Climate Change*, *12*(2), 171–178. https://doi.org/10.1038/s41558-021-01272-7

Gründemann, G. J., Zorzetto, E., Beck, H. E., Schleiss, M., Van De Giesen, N., Marani, M., & Van Der Ent, R. J. (2023). Extreme precipitation return levels for multiple durations on a global scale. *Journal of Hydrology*, *621*, 129558. https://doi.org/10.1016/j.jhydrol.2023.129558

Guzman, O., & Jiang, H. (2021). Global increase in tropical cyclone rain rate. *Nature Communications*, *12*(1), 5344. https://doi.org/10.1038/s41467-021-25685-2

Haarsma, R. J., Roberts, M. J., Vidale, P. L., Senior, C. A., Bellucci, A., Bao, Q., Chang, P., Corti, S., Fučkar, N. S., Guemas, V., Von Hardenberg, J., Hazeleger, W., Kodama, C., Koenigk, T., Leung, L. R., Lu, J., Luo, J.-J., Mao, J., Mizielinski, M. S., … Von Storch, J.-S. (2016). High Resolution Model Intercomparison Project (HighResMIP v1.0) for CMIP6. *Geoscientific Model Development*, *9*(11), 4185–4208. https://doi.org/10.5194/gmd-9-4185-2016

Hazeleger, W., Van Den Hurk, B. J. J. M., Min, E., Van Oldenborgh, G. J., Petersen, A. C., Stainforth, D. A., Vasileiadou, E., & Smith, L. A. (2015). Tales of future weather. *Nature Climate Change*, *5*(2), 107–113. https://doi.org/10.1038/nclimate2450

Henny, L., Thorncroft, C. D., & Bosart, L. F. (2023). Changes in Seasonal Large-Scale Extreme Precipitation in the Mid-Atlantic and Northeast United States, 1979–2019. *Journal of Climate*, *36*(4), 1017–1042. https://doi.org/10.1175/JCLI-D-22-0088.1

Howarth, M. E., Thorncroft, C. D., & Bosart, L. F. (2019). Changes in Extreme Precipitation in the Northeast United States: 1979–2014. *Journal of Hydrometeorology*, *20*(4), 673–689. https://doi.org/10.1175/JHM-D-18-0155.1

Huang, H., Patricola, C. M., Winter, J. M., Osterberg, E. C., & Mankin, J. S. (2021). Rise in Northeast US extreme precipitation caused by Atlantic variability and climate change. *Weather and Climate Extremes*, *33*, 100351. https://doi.org/10.1016/j.wace.2021.100351

Huang, H., Winter, J. M., & Osterberg, E. C. (2018). Mechanisms of Abrupt Extreme Precipitation Change Over the Northeastern United States. *Journal of Geophysical Research: Atmospheres*, *123*(14), 7179–7192. https://doi.org/10.1029/2017JD028136

Huprikar, A. S., Stansfield, A. M., & Reed, K. A. (2024). A storyline analysis of Hurricane Irma's precipitation under various levels of climate warming. *Environmental Research Letters*, *19*(1), 014004. https://doi.org/10.1088/1748-9326/ad0c89

Innocenti, S., Mailhot, A., Leduc, M., Cannon, A. J., & Frigon, A. (2019). Projected Changes in the Probability Distributions, Seasonality, and Spatiotemporal Scaling of Daily and Subdaily Extreme Precipitation Simulated by a 50-Member Ensemble Over Northeastern North America. *Journal of Geophysical Research: Atmospheres*, *124*(19), 10427–10449. https://doi.org/10.1029/2019JD031210

Intergovernmental Panel On Climate Change (Ipcc). (2023). *Climate Change 2021 – The Physical Science Basis: Working Group I Contribution to the Sixth Assessment Report of the Intergovernmental Panel on Climate Change* (1st ed.). Cambridge University Press. https://doi.org/10.1017/9781009157896

Irving, D. B., Risbey, J. S., Squire, D. T., Matear, R., Tozer, C., Monselesan, D. P., Ramesh, N., Reddy, P. J., & Freund, M. (2024). A multi-model likelihood analysis of unprecedented extreme rainfall along the east coast of Australia. *Meteorological Applications*, *31*(3), e2217. https://doi.org/10.1002/met.2217

Jeon, S., Paciorek, C. J., & Wehner, M. F. (2016). Quantile-based bias correction and uncertainty quantification of extreme event attribution statements. *Weather and Climate Extremes*, *12*, 24–32. https://doi.org/10.1016/j.wace.2016.02.001

Jones, A. D., Rastogi, D., Vahmani, P., Stansfield, A. M., Reed, K. A., Thurber, T., Ullrich, P. A., & Rice, J. S. (2023). Continental United States climate projections based on thermodynamic modification of historical weather. *Scientific Data*, *10*(1), 664. https://doi.org/10.1038/s41597-023-02485-5

Jong, B., Murakami, H., Delworth, T. L., & Cooke, W. F. (2024a). Contributions of Tropical Cyclones and Atmospheric Rivers to Extreme Precipitation Trends Over the Northeast US. *Earth's Future*, *12*(4), e2023EF004370. https://doi.org/10.1029/2023EF004370

Jong, B., Murakami, H., Delworth, T. L., & Cooke, W. F. (2024b). Contributions of Tropical Cyclones and Atmospheric Rivers to Extreme Precipitation Trends Over the Northeast US. *Earth's Future*, *12*(4), e2023EF004370. https://doi.org/10.1029/2023EF004370

Jong, B.-T., Delworth, T. L., Cooke, W. F., Tseng, K.-C., & Murakami, H. (2023). Increases in extreme precipitation over the Northeast United States using high-resolution climate model simulations. *Npj Climate and Atmospheric Science*, *6*(1), 18. https://doi.org/10.1038/s41612-023-00347-w

Jorgensen, S. K., & Nielsen-Gammon, J. W. (2024). Nonstationarity in Extreme Precipitation Return Values along the U.S. Gulf and Southeastern Coasts. *Journal of Hydrometeorology*, *25*(5), 771–788. https://doi.org/10.1175/JHM-D-22-0157.1

Kendall, M. (1948). *Rank correlation methods*. Griffin.

Kharin, V. V., Flato, G. M., Zhang, X., Gillett, N. P., Zwiers, F., & Anderson, K. J. (2018). Risks from Climate Extremes Change Differently from 1.5°C to 2.0°C Depending on Rarity. *Earth's Future*, *6*(5), 704–715. https://doi.org/10.1002/2018EF000813

Knutson, T., Camargo, S. J., Chan, J. C. L., Emanuel, K., Ho, C.-H., Kossin, J., Mohapatra, M., Satoh, M., Sugi, M., Walsh, K., & Wu, L. (2020). Tropical Cyclones and Climate Change Assessment: Part II: Projected Response to Anthropogenic Warming. *Bulletin of the American Meteorological Society*, *101*(3), E303–E322. https://doi.org/10.1175/BAMS-D-18-0194.1

Kolmogorov–Smirnov Test. (2008). In *The Concise Encyclopedia of Statistics* (pp. 283–287). Springer New York. https://doi.org/10.1007/978-0-387-32833-1_214

Kunkel, K. E., Easterling, D. R., Kristovich, D. A. R., Gleason, B., Stoecker, L., & Smith, R. (2010). Recent increases in U.S. heavy precipitation associated with tropical cyclones. *Geophysical Research Letters*, *37*(24), 2010GL045164. https://doi.org/10.1029/2010GL045164

Kunkel, K. E., Karl, T. R., Squires, M. F., Yin, X., Stegall, S. T., & Easterling, D. R. (2020). Precipitation Extremes: Trends and Relationships with Average Precipitation and Precipitable Water in the Contiguous United States. *Journal of Applied Meteorology and Climatology*, *59*(1), 125–142. https://doi.org/10.1175/JAMC-D-19-0185.1

Li, C., Sinha, E., Horton, D. E., Diffenbaugh, N. S., & Michalak, A. M. (2014). Joint bias correction of temperature and precipitation in climate model simulations. *Journal of Geophysical Research: Atmospheres*, *119*(23). https://doi.org/10.1002/2014JD022514

Lin, Y., & Mitchell, K. E. (2005). The NCEP stage II/IV hourly precipitation analyses: Development and applications. Preprints. *Preprints. 19th Conf. on Hydrology, San Diego, CA, Amer. Meteor. Soc., 1.2*. https://ams.confex.com/ams/pdfpapers/83847.pdf

Mann, H. B. (1945). Nonparametric Tests Against Trend. *Econometrica*, *13*(3), 245. https://doi.org/10.2307/1907187

Maraun, D. (2013). Bias Correction, Quantile Mapping, and Downscaling: Revisiting the Inflation Issue. *Journal of Climate*, *26*(6), 2137–2143. https://doi.org/10.1175/JCLI-D-12-00821.1

Martel, J.-L., Brissette, F. P., Lucas-Picher, P., Troin, M., & Arsenault, R. (2021). Climate Change and Rainfall Intensity–Duration–Frequency Curves: Overview of Science and Guidelines for Adaptation. *Journal of Hydrologic Engineering*, *26*(10), 03121001. https://doi.org/10.1061/(ASCE)HE.1943-5584.0002122

Martinez-Villalobos, C., & Neelin, J. D. (2023). Regionally high risk increase for precipitation extreme events under global warming. *Scientific Reports*, *13*(1), 5579. https://doi.org/10.1038/s41598-023-32372-3

Mehrotra, R., & Sharma, A. (2021). A robust alternative for correcting systematic biases in multi-variable climate model simulations. *Environmental Modelling & Software*, *139*, 105019. https://doi.org/10.1016/j.envsoft.2021.105019

Meinshausen, M., & Nicholls, Z. R. J. (2018). *UoM-REMIND-MAGPIE-ssp585-1-2-0: REMIND-MAGPIE-ssp585 GHG concentrations* (Version 20230213) [Application/x-netcdf]. Earth System Grid Federation. https://doi.org/10.22033/ESGF/INPUT4MIPS.2349

Meinshausen, M., & Vogel, E. (2016). *Input4MIPs.UoM.GHGConcentrations.CMIP.UoM-CMIP-1-2-0* (Version 20230220) [Application/x-netcdf]. Earth System Grid Federation. https://doi.org/10.22033/ESGF/INPUT4MIPS.1118

Menemenlis, S., Vecchi, G. A., Gao, K., Smith, J. A., & Cheng, K.-Y. (2024). Extreme Rainfall Risk in Hurricane Ida's Extratropical Stage: An Analysis with Convection-Permitting Ensemble Hindcasts. *Journal of the Atmospheric Sciences*, *81*(7), 1165–1179. https://doi.org/10.1175/JAS-D-23-0160.1

Menne, M. J., Durre, I., Vose, R. S., Gleason, B. E., & Houston, T. G. (2012). An Overview of the Global Historical Climatology Network-Daily Database. *Journal of Atmospheric and Oceanic Technology*, *29*(7), 897–910. https://doi.org/10.1175/JTECH-D-11-00103.1

Moradian, S., Gharbia, S., Torabi Haghighi, A., & Olbert, I. A. (2024). Modelling extreme precipitation projections under the effects of climate change: Case study of the Caspian Sea. *International Journal of Water Resources Development*, 1–21. https://doi.org/10.1080/07900627.2024.2400505

Mossel, C., Hill, S. A., Samal, N. R., Booth, J. F., & Devineni, N. (2024). Increasing extreme hourly precipitation risk for New York City after Hurricane Ida. *Scientific Reports*, *14*(1), 27947. https://doi.org/10.1038/s41598-024-78704-9

Moustakis, Y., Papalexiou, S. M., Onof, C. J., & Paschalis, A. (2021). Seasonality, Intensity, and Duration of Rainfall Extremes Change in a Warmer Climate. *Earth's Future*, *9*(3), e2020EF001824. https://doi.org/10.1029/2020EF001824

Murakami, H., Levin, E., Delworth, T. L., Gudgel, R., & Hsu, P.-C. (2018). Dominant effect of relative tropical Atlantic warming on major hurricane occurrence. *Science*, *362*(6416), 794–799. https://doi.org/10.1126/science.aat6711

Myhre, G., Alterskjær, K., Stjern, C. W., Hodnebrog, Ø., Marelle, L., Samset, B. H., Sillmann, J., Schaller, N., Fischer, E., Schulz, M., & Stohl, A. (2019). Frequency of extreme precipitation increases extensively with event rareness under global warming. *Scientific Reports*, *9*(1), 16063. https://doi.org/10.1038/s41598-019-52277-4

Nanditha, J. S., Villarini, G., Kim, H., & Naveau, P. (2024). Strong Linkage Between Observed Daily Precipitation Extremes and Anthropogenic Emissions Across the Contiguous United States. *Geophysical Research Letters*, *51*(20), e2024GL109553. https://doi.org/10.1029/2024GL109553

O'Gorman, P. A. (2015). Precipitation Extremes Under Climate Change. *Current Climate Change Reports*, *1*(2), 49–59. https://doi.org/10.1007/s40641-015-0009-3

Olafsdottir, H. K., Rootzén, H., & Bolin, D. (2021). Extreme rainfall events in the Northeastern USA become more frequent with rising temperatures, but their intensity distribution remains stable. *Journal of Climate*, 1–51. https://doi.org/10.1175/JCLI-D-20-0938.1

Olschewski, P., & Kunstmann, H. (2024). Future projections of hurricane intensity in the southeastern U.S.: Sensitivity to different Pseudo-Global Warming methods. *Frontiers in Climate*, *6*. https://doi.org/10.3389/fclim.2024.1353396

Paciorek, C. J., & Schervish, M. J. (2006). Spatial modelling using a new class of nonstationary covariance functions. *Environmetrics*, *17*(5), 483–506. https://doi.org/10.1002/env.785

Paciorek, C. J., Stone, D. A., & Wehner, M. F. (2018a). Quantifying statistical uncertainty in the attribution of human influence on severe weather. *Weather and Climate Extremes*, *20*, 69–80. https://doi.org/10.1016/j.wace.2018.01.002

Paciorek, C. J., Stone, D. A., & Wehner, M. F. (2018b). Quantifying statistical uncertainty in the attribution of human influence on severe weather. *Weather and Climate Extremes*, *20*, 69–80. https://doi.org/10.1016/j.wace.2018.01.002

Peduzzi, P., Chatenoux, B., Dao, H., De Bono, A., Herold, C., Kossin, J., Mouton, F., & Nordbeck, O. (2012). Global trends in tropical cyclone risk. *Nature Climate Change*, *2*(4), 289–294. https://doi.org/10.1038/nclimate1410

Pendergrass, A. G., & Knutti, R. (2018). The Uneven Nature of Daily Precipitation and Its Change. *Geophysical Research Letters*, *45*(21). https://doi.org/10.1029/2018GL080298

Perkins-Kirkpatrick, S. E., Stone, D. A., Mitchell, D. M., Rosier, S., King, A. D., Lo, Y. T. E., Pastor-Paz, J., Frame, D., & Wehner, M. (2022). On the attribution of the impacts of extreme weather events to anthropogenic climate change. *Environmental Research Letters*, *17*(2), 024009. https://doi.org/10.1088/1748-9326/ac44c8

Prein, A. F., Rasmussen, R. M., Ikeda, K., Liu, C., Clark, M. P., & Holland, G. J. (2017). The future intensification of hourly precipitation extremes. *Nature Climate Change*, *7*(1), 48–52. https://doi.org/10.1038/nclimate3168

Ragno, E., AghaKouchak, A., Love, C. A., Cheng, L., Vahedifard, F., & Lima, C. H. R. (2018). Quantifying Changes in Future Intensity-Duration-Frequency Curves Using Multimodel Ensemble Simulations. *Water Resources Research*, *54*(3), 1751–1764. https://doi.org/10.1002/2017WR021975

Rahat, S. H., Saki, S., Khaira, U., Biswas, N. K., Dollan, I. J., Wasti, A., Miura, Y., Bhuiyan, M. A. E., & Ray, P. (2024). Bracing for impact: How shifting precipitation extremes may influence physical climate risks in an uncertain future. *Scientific Reports*, *14*(1), 17398. https://doi.org/10.1038/s41598-024-65618-9

Rasmussen, R., & Liu, C. (2017). *High Resolution WRF Simulations of the Current and Future Climate of North America* (p. 192.795 Tbytes) [NetCDF4]. UCAR/NCAR - Research Data Archive. https://doi.org/10.5065/D6V40SXP

Reed, K. A., Stansfield, A. M., Wehner, M. F., & Zarzycki, C. M. (2020). Forecasted attribution of the human influence on Hurricane Florence. *Science Advances*, *6*(1), eaaw9253. https://doi.org/10.1126/sciadv.aaw9253

Reed, K. A., & Wehner, M. F. (2023). Real-time attribution of the influence of climate change on extreme weather events: A storyline case study of Hurricane Ian rainfall. *Environmental Research: Climate*, *2*(4), 043001. https://doi.org/10.1088/2752-5295/acfd4e

Risser, M. D., Collins, W. D., Wehner, M. F., O'Brien, T. A., Huang, H., & Ullrich, P. A. (2024). Anthropogenic aerosols mask increases in US rainfall by greenhouse gases. *Nature Communications*, *15*(1), 1318. https://doi.org/10.1038/s41467-024-45504-8

Risser, M. D., Collins, W. D., Wehner, M. F., O'Brien, T. A., Paciorek, C. J., O'Brien, J. P., Patricola, C. M., Huang, H., Ullrich, P. A., & Loring, B. (2023a). A framework for detection and attribution of regional precipitation change: Application to the United States historical record. *Climate Dynamics*, *60*(3–4), 705–741. https://doi.org/10.1007/s00382-022-06321-1

Risser, M. D., Collins, W. D., Wehner, M. F., O'Brien, T. A., Paciorek, C. J., O'Brien, J. P., Patricola, C. M., Huang, H., Ullrich, P. A., & Loring, B. (2023b). A framework for detection and attribution of regional precipitation change: Application to the United States historical record. *Climate Dynamics*, *60*(3–4), 705–741. https://doi.org/10.1007/s00382-022-06321-1

Risser, M. D., Paciorek, C. J., Wehner, M. F., O'Brien, T. A., & Collins, W. D. (2019). A probabilistic gridded product for daily precipitation extremes over the United States. *Climate Dynamics*, *53*(5–6), 2517–2538. https://doi.org/10.1007/s00382-019-04636-0

Roberts, M. J., Reed, K. A., Bao, Q., Barsugli, J. J., Camargo, S. J., Caron, L.-P., Chang, P., Chen, C.-T., Christensen, H. M., Danabasoglu, G., Frenger, I., Fučkar, N. S., Ul Hasson, S., Hewitt, H. T., Huang, H., Kim, D., Kodama, C., Lai, M., Leung, L.-Y. R., … Zhao, M. (2025). High-Resolution Model Intercomparison Project phase 2 (HighResMIP2) towards CMIP7. *Geoscientific Model Development*, *18*(4), 1307–1332. https://doi.org/10.5194/gmd-18-1307-2025

Schär, C., Frei, C., Lüthi, D., & Davies, H. C. (1996). Surrogate climate-change scenarios for regional climate models. *Geophysical Research Letters*, *23*(6), 669–672. https://doi.org/10.1029/96GL00265

Sen, P. K. (1968). Estimates of the Regression Coefficient Based on Kendall's Tau. *Journal of the American Statistical Association*, *63*(324), 1379–1389. https://doi.org/10.1080/01621459.1968.10480934

Serinaldi, F., & Kilsby, C. G. (2015). Stationarity is undead: Uncertainty dominates the distribution of extremes. *Advances in Water Resources*, *77*, 17–36. https://doi.org/10.1016/j.advwatres.2014.12.013

Sharif, R. B., Habib, E. H., & ElSaadani, M. (2020). Evaluation of Radar-Rainfall Products over Coastal Louisiana. *Remote Sensing*, *12*(9), 1477. https://doi.org/10.3390/rs12091477

Shepherd, T. G., Boyd, E., Calel, R. A., Chapman, S. C., Dessai, S., Dima-West, I. M., Fowler, H. J., James, R., Maraun, D., Martius, O., Senior, C. A., Sobel, A. H., Stainforth, D. A., Tett, S. F. B., Trenberth, K. E., Van Den Hurk, B. J. J. M., Watkins, N. W., Wilby, R. L., & Zenghelis, D. A. (2018). Storylines: An alternative approach to representing uncertainty in physical aspects of climate change. *Climatic Change*, *151*(3–4), 555–571. https://doi.org/10.1007/s10584-018-2317-9

Slater, L. J., Anderson, B., Buechel, M., Dadson, S., Han, S., Harrigan, S., Kelder, T., Kowal, K., Lees, T., Matthews, T., Murphy, C., & Wilby, R. L. (2021). Nonstationary weather and water extremes: A review of methods for their detection, attribution, and management. *Hydrology and Earth System Sciences*, *25*(7), 3897–3935. https://doi.org/10.5194/hess-25-3897-2021

Smith, J. A., Baeck, M. L., Su, Y., Liu, M., & Vecchi, G. A. (2023). Strange Storms: Rainfall Extremes From the Remnants of Hurricane Ida (2021) in the Northeastern US. *Water Resources Research*, *59*(3), e2022WR033934. https://doi.org/10.1029/2022WR033934

Srivastava, A. K., Ullrich, P. A., Rastogi, D., Vahmani, P., Jones, A., & Grotjahn, R. (2023). Assessment of WRF (v 4.2.1) dynamically downscaled precipitation on subdaily and daily timescales over CONUS. *Geoscientific Model Development*, *16*(13), 3699–3722. https://doi.org/10.5194/gmd-16-3699-2023

Stansfield, A. M., Reed, K. A., & Zarzycki, C. M. (2020). Changes in Precipitation From North Atlantic Tropical Cyclones Under RCP Scenarios in the Variable-Resolution Community Atmosphere Model. *Geophysical Research Letters*, *47*(12), e2019GL086930. https://doi.org/10.1029/2019GL086930

Tanaka, T., Kawase, H., Imada, Y., Kawai, Y., & Watanabe, S. (2023). Risk-based versus storyline approaches for global warming impact assessment on basin-averaged extreme rainfall: A case study for Typhoon Hagibis in eastern Japan. *Environmental Research Letters*, *18*(5), 054010. https://doi.org/10.1088/1748-9326/accc24

Theil, H. (1950). A rank-invariant method of linear and polynomial regression analysis, 1-2; confidence regions for the parameters of linear regression equations in two, three and more variables. *Stichting Mathematisch Centrum*, *1950-01–01*. https://ir.cwi.nl/pub/18445

Timmermans, B., Wehner, M., Cooley, D., O'Brien, T., & Krishnan, H. (2019). An evaluation of the consistency of extremes in gridded precipitation data sets. *Climate Dynamics*, *52*(11), 6651–6670. https://doi.org/10.1007/s00382-018-4537-0

Tyralis, H., Papacharalampous, G., & Tantanee, S. (2019). How to explain and predict the shape parameter of the generalized extreme value distribution of streamflow extremes using a big dataset. *Journal of Hydrology*, *574*, 628–645. https://doi.org/10.1016/j.jhydrol.2019.04.070

Uehling, J., & Schreck, C. J. (2024). Observed Changes in Extreme Precipitation Associated with U.S. Tropical Cyclones. *Journal of Climate*, *37*(14), 3661–3674. https://doi.org/10.1175/JCLI-D-23-0327.1

Van Der Wiel, K., Kapnick, S. B., Van Oldenborgh, G. J., Whan, K., Philip, S., Vecchi, G. A., Singh, R. K., Arrighi, J., & Cullen, H. (2017). Rapid attribution of the August 2016 flood-inducing extreme precipitation in south Louisiana to climate change. *Hydrology and Earth System Sciences*, *21*(2), 897–921. https://doi.org/10.5194/hess-21-897-2017

Vasiliades, L., Galiatsatou, P., & Loukas, A. (2015). Nonstationary Frequency Analysis of Annual Maximum Rainfall Using Climate Covariates. *Water Resources Management*, *29*(2), 339–358. https://doi.org/10.1007/s11269-014-0761-5

Villarini, G., & Smith, J. A. (2010). Flood peak distributions for the eastern United States. *Water Resources Research*, *46*(6), 2009WR008395. https://doi.org/10.1029/2009WR008395

Vohnicky, P., Dallan, E., Marra, F., Fosser, G., & Borga, M. (2025). Future precipitation extremes: Differential changes from point to catchment scale revealed by a convection-permitting model ensemble. *Journal of Hydrology*, *662*, 133822. https://doi.org/10.1016/j.jhydrol.2025.133822

Vu, T. M., & Mishra, A. K. (2019). Nonstationary frequency analysis of the recent extreme precipitation events in the United States. *Journal of Hydrology*, *575*, 999–1010. https://doi.org/10.1016/j.jhydrol.2019.05.090

Wang, S., & Wang, Y. (2019). Improving probabilistic hydroclimatic projections through high-resolution convection-permitting climate modeling and Markov chain Monte Carlo simulations. *Climate Dynamics*, *53*(3–4), 1613–1636. https://doi.org/10.1007/s00382-019-04702-7

Wang, X., Huang, G., & Liu, J. (2014). Projected increases in intensity and frequency of rainfall extremes through a regional climate modeling approach. *Journal of Geophysical Research: Atmospheres*, *119*(23). https://doi.org/10.1002/2014JD022564

Wehner, M. F., Reed, K. A., Loring, B., Stone, D., & Krishnan, H. (2018). Changes in tropical cyclones under stabilized 1.5 and 2.0 °C global warming scenarios as simulated by the Community Atmospheric Model under the HAPPI protocols. *Earth System Dynamics*, *9*(1), 187–195. https://doi.org/10.5194/esd-9-187-2018

Wright, D. B., Knutson, T. R., & Smith, J. A. (2015). Regional climate model projections of rainfall from U.S. landfalling tropical cyclones. *Climate Dynamics*, *45*(11–12), 3365–3379. https://doi.org/10.1007/s00382-015-2544-y

Zarzycki, C. M., Zhang, T., Jones, A. D., Rastogi, D., Vahmani, P., & Ullrich, P. A. (2024). Changes in Four Decades of Near-CONUS Tropical Cyclones in an Ensemble of 12 km Thermodynamic Global Warming Simulations. *Geophysical Research Letters*, *51*(18). https://doi.org/10.1029/2024gl110535

Zorzetto, E., Botter, G., & Marani, M. (2016). On the emergence of rainfall extremes from ordinary events. *Geophysical Research Letters*, *43*(15), 8076–8082. https://doi.org/10.1002/2016GL069445